

POLITECNICO DI TORINO

Collegio di Ingegneria Chimica e dei Materiali

**Master of Science Course  
in Materials Engineering**

Master of Science Thesis

**"Influence of CNTs functionalization on the mechanical and  
electrical properties of cement-based composites."**



**Tutors**

Prof. Pavese Matteo

Dott. Lavagna Luca

**Candidate**

Cagliero Davide

MARCH 2021



# CONTENTS

<b>1. INTRODUCTION .....</b>	<b>5</b>
<b>2. PROPERTIES OF CARBON NANOTUBES .....</b>	<b>6</b>
<b>2.1 Carbon and its allotropes .....</b>	<b>6</b>
2.1.1 Diamond .....	6
2.1.2 Graphite .....	7
<b>2.2 Carbon nanotubes .....</b>	<b>8</b>
2.2.1 Single Wall Carbon Nanotubes .....	9
2.2.2 Multi Wall Carbon Nanotubes .....	10
<b>2.3 Carbon Nanotubes synthesis processes .....</b>	<b>11</b>
2.3.1 Arc Discharge Method .....	11
2.3.2 Laser Ablation .....	12
2.3.3 Chemical Vapor Deposition .....	13
2.3.4 Plasma Enhanced CVD .....	14
<b>2.4 Carbon Nanotubes applications .....</b>	<b>15</b>
2.4.1 Nanocomposites material .....	15
2.4.2 Coatings and films .....	16
2.4.3 Microelectronic devices .....	17
2.4.4 Energy storage .....	18
2.4.5 Biotechnology .....	19
<b>3. CEMENT .....</b>	<b>20</b>
<b>3.1 Production of Portland cement .....</b>	<b>20</b>
<b>3.2 Hydration process of Portland cement .....</b>	<b>23</b>

<b>3.3 Effect of Carbon nanotubes on cement hydration and flowability .....</b>	<b>29</b>
<b>4. CARBON NANOTUBES FUNCTIONALIZATION .....</b>	<b>34</b>
<b>4.1 Non-covalent functionalization .....</b>	<b>35</b>
<b>4.2 Covalent functionalization .....</b>	<b>35</b>
<b>6. MATERIALS AND METHODS .....</b>	<b>36</b>
<b>6.1 Carbon Nanotubes characterization .....</b>	<b>36</b>
6.1.1 Thermogravimetric Analysis .....	36
6.1.2 Raman Spectroscopy .....	38
6.1.2.1 Theory of Raman spectroscopy .....	38
6.1.2.2 Conventional Raman instrument .....	40
<b>6.2 Carbon Nanotubes Functionalization .....</b>	<b>41</b>
<b>6.3 CNTs-Cement Composites .....</b>	<b>44</b>
6.3.1 CNTs-cement composites production .....	44
6.3.2 Geometrical Density .....	47
6.3.3 Resistivity .....	48
<b>6.4 Mechanical Tests on CNTs-Cement Composites .....</b>	<b>51</b>
6.4.1 Three-point flexural test .....	51
6.4.2 Compressive tests .....	54
<b>7. RESULTS AND DISCUSSION .....</b>	<b>55</b>
<b>8. CONCLUSIONS .....</b>	<b>74</b>

## 1. INTRODUCTION

Nanotechnology has changed and will continue to change our vision, expectations and abilities to control the material world. These developments are going to play a massive role in the field of construction and construction materials. Carbon nanotubes (CNTs) are considered to be one of the most beneficial nano-reinforcement materials. The combination of high aspect ratio, small size, low density, and unique physical and chemical properties make them perfect candidates as reinforcements in multifunctional and smart cement-based materials.

In the construction sector, attention and exploration in the field of carbon-based materials have been ongoing for many years. Although carbon fibers have already been applied to cementitious composites, carbon nanotubes (CNTs), as nanomaterials, have received widespread attention as a result of their unique multifunctional properties within the context of engineered materials, regarding both the mechanical and electrical properties of the composites. The main task of the present work is to evaluate and comprehend the changes in mechanical and electrical properties of several CNT-cement-based composite containing 0,1% by weight of cement of carbon nanotubes, in which the CNTs are modified with a functionalization process for grafting oxygenated functional groups on their surfaces. The effects of functionalization time were evaluated in order to improve the mechanical properties and reduce the cement resistivity. The functionalization process was conducted with the desire to identify the possible improvements caused by the interaction between the carbon nanotubes and the cement matrix, especially the effect of the oxygenated groups attached on the CNTs surface.

This type of composite material can be seen as an optimal sensing material that can be used to monitor the structures and buildings, preventing serious accidents.

## 2.1 CARBON AND ITS ALLOTROPES

Carbon is a chemical element with the symbol C and an atomic number of 6. It is a non-metallic element and has a high affinity to form bonds with low atomic weight atoms; in addition to this, carbon exhibits the very important property of forming bonds with itself creating various allotropic forms such as diamond, graphite, fullerene and carbon nanotubes. The carbon atom can show three types of hybridization:  $sp^3$ ,  $sp^2$ , and  $sp$ ; thanks to these types of hybridization, carbon is able to bind to another 4, 3 and 2 carbon atoms respectively (the bond angle of tetragonal geometry is  $109.5^\circ$ , that of trigonal geometry is  $120^\circ$  and finally the respective angle to planar geometry is  $180^\circ$ ). Its stability and willingness to create strong covalent bonds with other atoms make carbon capable of forming long chains of atoms that turn out to be fundamental for the development of organic molecules. Carbon is present in nature under two allotropic forms: graphite and diamond.

### 2.1.1 DIAMOND

Diamond is an allotropic form of carbon in which carbon atoms form an orderly tetrahedral structure through strong covalent bonds. This type of structure allows an exclusive combination of mechanical, physical and electrical properties. The most important properties to mention are in fact the very high hardness, the excellent thermal conductivity and the excellent chemical inertia. Due to its high hardness, diamond is mainly used as a coating for cutting tools for ceramic materials. As for the breaking load of the diamond, a load of 60 GPa has been observed, but that can reach up to a maximum of 200 GPa in case we are in the presence of a perfect crystal lattice. In addition, the highest breaking load is demonstrated at the crystalline direction [100]. Diamond is an insulating material, but unlike most insulating materials, diamond is an excellent heat conductor thanks firstly to the strong covalent bonds that characterize its crystalline structure, and secondly thanks to the limited phonon scattering within the crystal. It shows thermal conductivity values of around  $2200 \text{ W}/(\text{m}\cdot\text{K})$ . In nature, diamond synthesis takes place under particularly drastic conditions, i.e. at pressures not less than 5-6 GPa and at temperatures above  $1000^\circ\text{C}$ . However, there is also an industrial method widely used for diamond synthesis, namely chemical vapour deposition (CVD) [1].

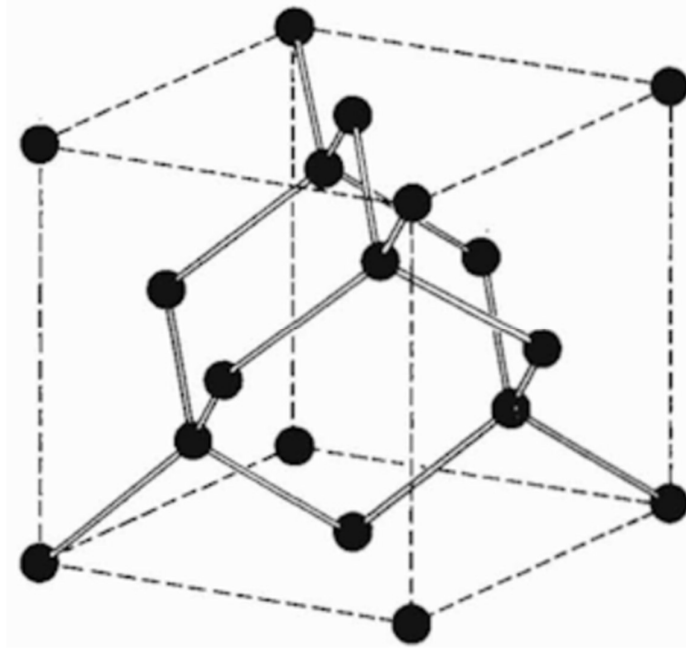


*Figure 1. Structure of diamond lattice*

### **2.1.2 GRAPHITE**

The graphite structure consists of planar layers of carbon atoms, in which each carbon is bound in a planar configuration to another 3 carbon atoms by sigma bonds with  $sp^2$  hybridization to form a hexagonal structure. The layers, on the other hand, are bound together by Van der Waals forces. This causes the structure to have very strong intralayer bonds, on the contrary very weak interlayer bonds [2]. The main advantage due to this type of interaction between carbon atoms is that it shows itself as a very interesting solid lubricant due to the fact that the planes can slide between them. The interlayer distance, i.e. the distance separating 2 carbon atoms belonging to 2 layers of adjacent graphene, is about 3.36 Å, while the intraplanar bond distance, i.e. the distance of the covalent bond between two carbon atoms of the same layer is about 1.42 Å [3].

### **2.2 CARBON NANOTUBES**

Continuous research in the field of carbon chemistry allowed Japanese scientist Sumio Iijima to observe the structure of carbon nanotubes for the first time in 1991 [4]. Although the greatest credit has been given to researcher Iijima, the first appearance in the Journal of Physical

Chemistry of Russia of carbon nanotubes dates to 1952, thanks to the work of a team of Russian researchers [5]. This was also achieved thanks to the invention of the Transmission Electron Microscope in 1939, which allowed significant advances in the characterization of carbon filament morphology. Due to political issues during the Cold War period, however, access to Soviet scientific publications was very complicated for Western researchers.

The results of continuous research in this field show that carbon nanotubes behave like graphene sheet cylinders of carbon atoms bound  $sp^2$ , at the end of which they are closed by two hemispherical caps (end caps) which, when joined together, form a fullerene [6]. This type of cylindrical geometry allows nanotubes to exhibit very important mechanical, electrical and thermal properties. Just think that the tensile strength of an ideal nanotube is 100 times higher than a steel bar, even though the specific weight of the nanotube is 6 times lower than the latter. In fact, it can be noted that if you relate the properties.

A general feature of nanotubes, which concerns its symmetry in space, is that the length of the tube turns out to be much larger than the diameter of the same, therefore, this allows to neglect the two "end caps" when discussing mechanical properties.

As for electrical conduction, carbon nanotubes show the interesting property that conductivity can be both metallic and semiconductor, both dependent on the nanotube diameter ( $d$ ) and its chiral angle ( $\theta$ ). In addition, for carbon nanotubes, metal conductivity can be achieved simply without the introduction of a doping chemical species or defects in the structure [7].

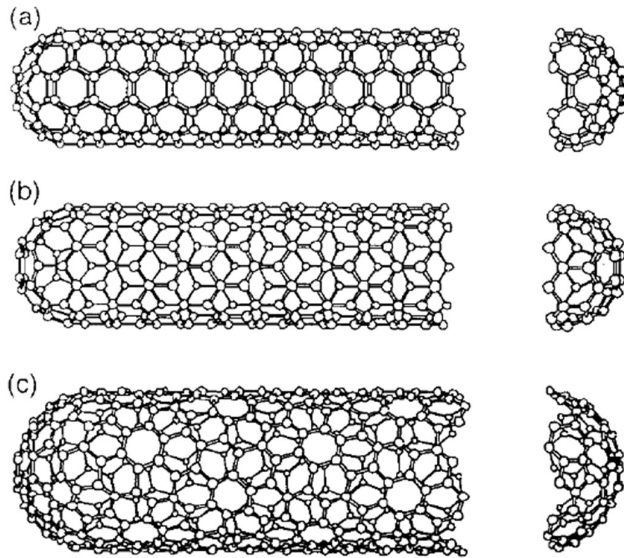


**Figure 2.** Schematic representation of different type of Carbon nanotubes structures

In general, nanotubes can be divided into 2 large families:

1. SWCNT (Single Wall Carbon Nano Tubes)
2. MWCNT (Multi Wall Carbon Nano Tubes)

The first consist of a single sheet of graphite wrapped on itself; the latter, on the other hand, consist of 2 or more sheets of graphite wrapped on the surface of the other.

### 2.2.1 SWCNT – SINGLE WALL CARBON NANOTUBES

The two main parameters needed to characterize the geometry of a single wall carbon nanotube are the tubular diameter ( $d$ ) and the chiral angle ( $\vartheta$ ). The combination of these two parameters allows to introduce another variable called chiral vector ( $C_h$ ), which is described by two terms of the two-base vector of the graphite lattice and forms the nanotube structure ( $a_1$  and  $a_2$ ) [8]. Moreover, the length of the chiral vector  $C_h$  seems to be directly related to the size of the tubular diameter  $d$ . It can be said that a single wall carbon nanotube derives from the cut along the bisector of a  $C_{60}$  on the equator and, after that, by putting together the 2 hemispheres obtained by a cylindric tube that has the same diameter of the  $C_{60}$  fullerene molecule, whose molecular structure is similar to the structure of a single graphite sheet (graphite layer) [9].

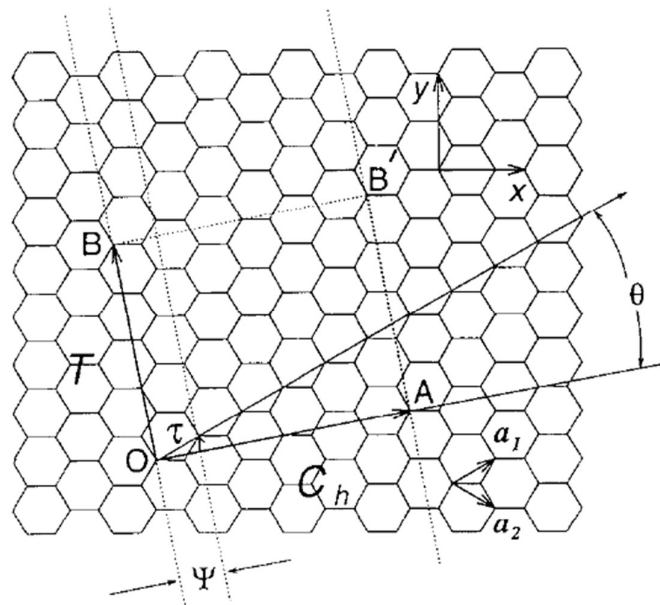


**Figure 3.** Representation of chiral vector and chiral angle for a SWCNT

### 2.2.2 MWCNT – MULTI WALL CARBON NANOTUBES

MWCNTs consists of two or more concentric cylindrical shells of graphene sheets with a layer spacing of 0,3-0,4 nm, coaxially arranged around a central hollow core. They show a high aspect ratio, low bulk density and an extended specific area, which is of particular interest for adsorption and reactions taking place on the nanotubes surface [10]. MWCNTs are inherently more complex than SWCNTs. There are innumerate configurations from the basic graphene building block. The simplest arrangement involves a concentric geometry in which successive tubes increase in diameter. Smaller tubes are contained within in turn into larger ones. MWCNTs have several walls, which may vary from 2 to an unlimited upper limit.

The diameter between tube walls within the MWCNT was measured and is approximately 0,34 nm [11]. The carbon atoms of graphene are positioned either opposite to one another or opposite carbon atoms from the neighboring graphene.

The herringbone is another common structure of MWCNTs. Structurally, two graphene sheets are arranged at an angle with respect to the nanotube axis. The size of this angle is dependent upon the exact processing conditions employed for the synthesis, such as composition and the catalyst used.

Multi-wall CNTs have an aspect ratio much lower than the SWCNTs and the ends can often be viewed with a TEM (Transmission Electron Microscope). The properties of MWCNTs are highly dependent on the perfection and orientations of graphene in the tubes [12].

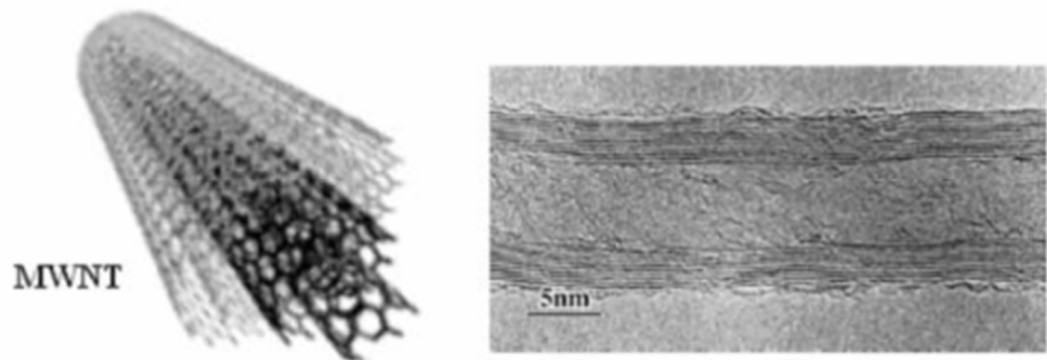


*Figure 4. SEM image showing several walls of size of 5nm for a MWCNT*

## **2.3 CARBON NANOTUBES SYNTHESIS PROCESSES**

In recent years, the production of carbon nanotubes in terms of volume produced has increased considerably, and the number of scientific publications related to CNTs continues to grow year after year; this continuous growth has led, therefore, to consider different synthesis methods for carbon nanotubes. The main synthesis methods that cover most of the production of nanotubes are the arc discharge method, laser ablation, Chemical Vapour Deposition, Electrolysis.

### **2.3.1 ARC DISCHARGE METHOD**

This is the method used by Iijima for the preparation of carbon nanotubes. This method involves the formation of nanotubes by creating a hot plasma by discharge between 2 graphite electrodes, which are connected to an electrical source of 100 A and 20 V; The atmosphere most used for this type of production is the He. Due to the high temperatures that can be reached in the chamber, which can reach more than 4000°C, there is the sublimation of the graphite anode and the

subsequent deposition to the graphite cathode in the form of carbon nanotubes and graphene. In accordance with the studies carried out by the Norwegian researcher T.W. Esseben and his Indian colleague P.M. Ajayan, the increase to a critical value of the pressure in the chamber, leads to a consequent increase in the yield of carbon nanotubes. However, the continuous increase in pressure and the exceeding of the critical threshold, leads to a drastic decrease in the yield of nanotubes. However, the increase in the quality of nanotubes depends on the decrease in the current that reaches the electrodes [13]. In addition, other gases can be used as an alternative to He such as, N<sub>2</sub> or CF<sub>4</sub> [14], since the use of organic vapors (such as CF<sub>4</sub>) increases the production yield of nanotubes.

### 2.3.2 LASER ABLATION

In this method the carbon source (which is graphite) needs to be doped with a very small amounts of metallic catalyst, which is then vaporized with the help of a pulsed laser beam in the presence of an atmosphere made by an inert gas (typically Ar is used), at very high temperatures (above 1200°C) and at a constant pressure of 0,66 atm. The laser beam is a Nd:YAG (Nd:Y<sub>3</sub>Al<sub>5</sub>O<sub>12</sub>) laser which consists of a crystal of yttrium aluminum garnet which is doped by a triply ionized neodymium (Nd(III)); in this case the neodymium ion provides the lasing activity in the crystal, similarly as red chromium ion in a ruby laser. As the Nd:YAG laser beam impregnates the target material, which in this case is the graphite, it starts vaporizing and condenses on the other end which is at comparatively lower temperature. The vaporization yield can increase by using a double pulsed laser, so that the production of the CNT's can go up to 1g/day. However, the fact that the requirements for this process are a high-power usage and employability of expensive lasers, this synthesis way results very costly In terms of money investment [15].

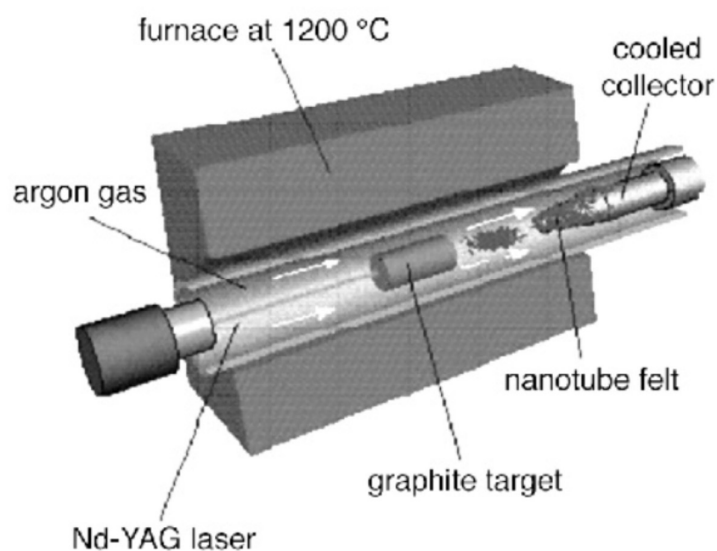


**Figure 5.** Scheme of a laser ablation method for the synthesis of carbon nanotubes

### 2.3.3 CHEMICAL VAPOR DEPOSITION

The chemical Vapor Deposition (CVD) process consists of the decomposition of reactant gases which form a solid product. Regarding the synthesis of carbon nanotubes [16], this method takes place due to the decomposition of a mixture of hydrocarbon gases (like methane, ethylene...) or volatile carbon compounds present in the reaction chamber onto a metallic substrate. The nanoparticles of the metallic substrate behave as catalysts and nucleation sites in the growth process of carbon nanotubes at temperatures that range between 500 and 1000°C and under atmospheric pressure. The selection of the catalyst and the preparation of the substrate decides the type and the quality of the nanotubes produced. Usually the catalyst nanoparticles used in this process are Fe, Co or Ni [17] [18]. Porous silicon is considered as an ideal substrate for controlled growth of the carbon nanotubes. In 2002, two scientists Govindaraj and Rao used organometallic compounds instead of hydrocarbon gases for the synthesis of CNT [19]. The main advantage of using organometallic compounds is that there is no requirement of the removal of the catalyst support after the reaction due to the presence of same phase of carbon source and catalyst simultaneously. Further modifications were done in this technique. The best one is the introduction of the Plasma Enhanced Chemical Vapor Deposition (PECVD), which is the most widely used method for CNT synthesis. This technique was first studied by Ren in 1998 [20]. In this

process, in fact, a DC plasma is used to guarantee the alignment of the carbon nanotubes. This technique is basically used for the fabrication of CNT based flat panels displays and solar cells [21]. Anyway, the use of low-cost feedstocks, the reduction of energy consumption and waste production, have substantially decreased MWNT prices [22]. However, large-scale CVD methods yield contaminants that can influence CNT properties and often require costly thermal annealing and a chemical treatment for their removal. So, these steps can introduce defects in CNT sidewalls and shorten CNT length [23].

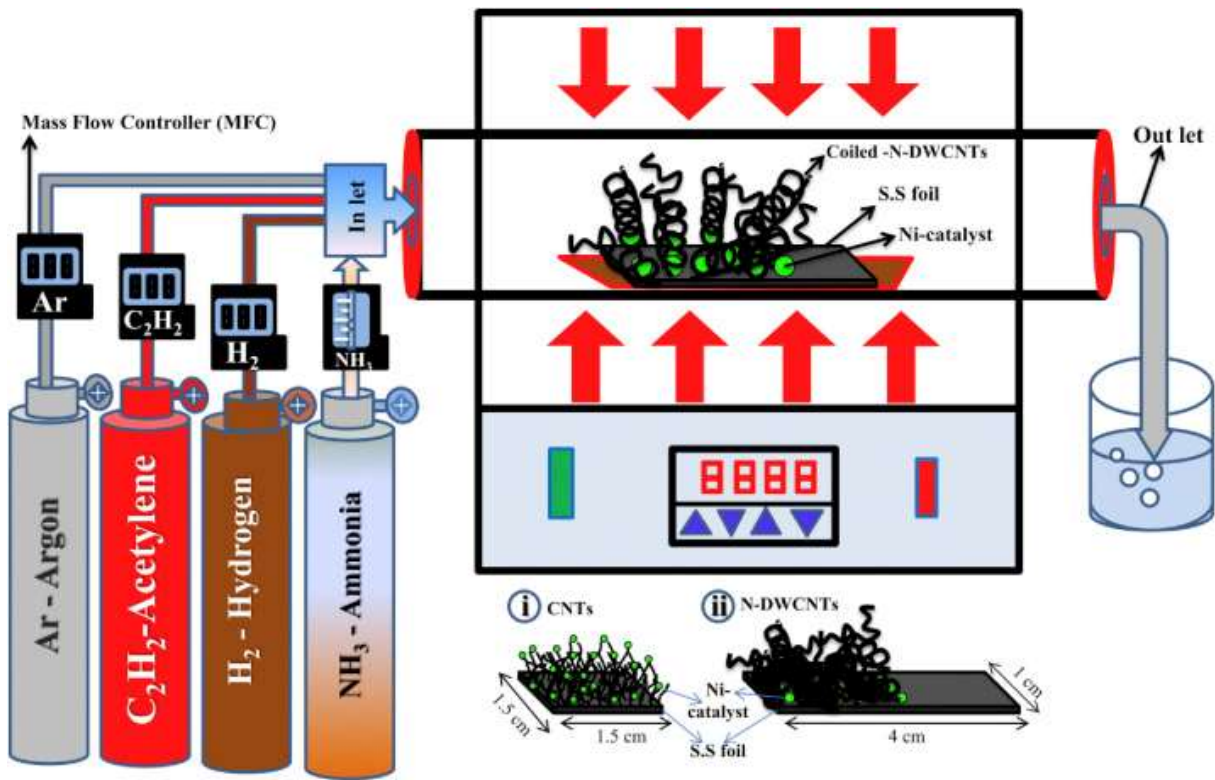
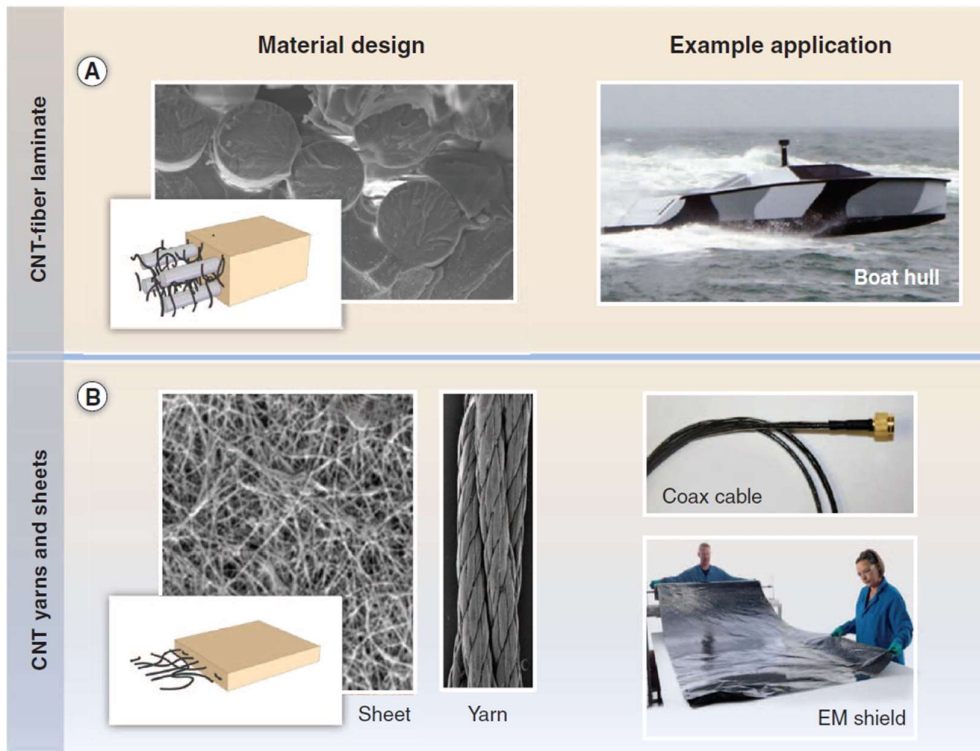


Figure 6. Chemical Vapor Deposition process for the synthesis of MWCNTs

## 2.4 CARBON NANOTUBES APPLICATIONS

### 2.4.1 NANOCOMPOSITES MATERIALS

MWCNT were first used as electrically conductive fillers in plastic, taking advantage of their high aspect ratio to form a percolation network as concentrations as low as 0,01 – 0,05 weight percent (%w). Adding 1 wt% to epoxy resins enhances stiffness and fracture toughness by 6 and 20 % respectively, without compromising the others mechanical properties. These enhancements depend on CNT diameter, aspect ratio, alignment, dispersion and interfacial interaction with the matrix [24]. High-performance fibers of aligned SWCNTs can be made by coagulation-based spinning of CNT suspensions [25]. This process is attractive for scale-up if the cost of high-quality SWCNTs decreases substantially or if spinning can be extended to low-cost MWCNTs. Thousands of spinnerets could operate in parallel and CNT orientation can be achieved via liquid crystal formation, like for the spinning of Kevlar. Besides polymer composites, the addition of a small amount of CNT's to metals has provided an increasing in tensile strength and modulus, that may find applications in aerospace and automotive structures. Commercial Al-MWNT composites have strengths comparable to stainless steel (0,8-1 GPa) at on third of his density ( $2,6 \text{ g cm}^{-3}$ ). The strength of these composites is also comparable to Al-Li alloys, yet the Al-MWCNT are still reported as a less expensive alternative. MWCNTs are also very interesting when used as a flame-retardant additive to plastics; this effect is mainly attributed to changes in rheology by nanotube loading. These nanotubes additives are commercially attractive as a replacement for halogenated flame retardants, which have restricted use due to the environmental regulations [26].



**Figure 7.** CNTs applications in composite materials [ ]

#### 2.4.2 COATINGS AND FILMS

Another interesting application for the CNTs is represented by their usage as an additive for several coatings and film. For example, MWCNTs-containing paints are a possible alternative to environmentally hazardous biocide-containing paints. Incorporation of Carbon nanotubes in anticorrosion coatings for metals can enhance very good stiffness and strength while providing an electrical pathway for cathodic protection [27]. The latest developments regarding CNTs as a dispersed phase in coatings showed that CNT-based transparent conducting films can be used as an alternative to Indium Tin Oxide (ITO) [28]. The main concern is that ITO is becoming more expensive because of the scarcity of Indium and also due to the fact that the demand for displays, touch-screen devices and photovoltaics is growing exponentially. Besides cost, the flexibility of CNT transparent conductors seems to be a major advantage over brittle ITO coatings. In fact, transparent nanotubes conductors can be deposited from solution (ultrasonic spraying) and patterned by cost-effective non-lithographic methods like screen printing or micro plotting. Recent

studies showed that SWCNTs films have about 90% transparency and a sheet resistivity of 100 ohm per square. Anyway, this surface resistivity is still substantially higher than for equally transparent Indium Tin Oxide coatings [29].

### 2.4.3 MICROELECTRONIC DEVICES

High-quality SWCNTs are very attractive for transistors because of their low electron scattering and their interesting band gap, which depends on diameter and chiral angle. Despite the promising performance of individual SWCNTs devices, control of the nanotube diameter, chirality, density and placement remains insufficient for microelectronics production [30]. Recent researches show that devices such as transistors with patterned films of tens of thousands of CNT arrays increases output current and compensates for defects and chirality differences on nanotubes and also improves device uniformity and reproducibility [31]. CNT thin-film transistors (TFTs) result particularly attractive for Organic Light-Emitting Diode (OLED) displays, because they have shown higher mobility than amorphous silicon ( $1 \text{ cm}^2\text{V}^{-1}\text{s}^{-1}$ ) and can be deposited by easier techniques with low temperatures and without a vacuum. Promising commercial development of CNTs electronics includes low-cost printing of TFTs. The International Technology Roadmap for Semiconductors suggests that carbon nanotubes could replace Cu in microelectronic interconnects due to their low scattering, high current-carrying capacity, and an optimal resistance to electromigration. However, for this type of application, metallic CNTs with low defect density and low contact resistance are needed [32].

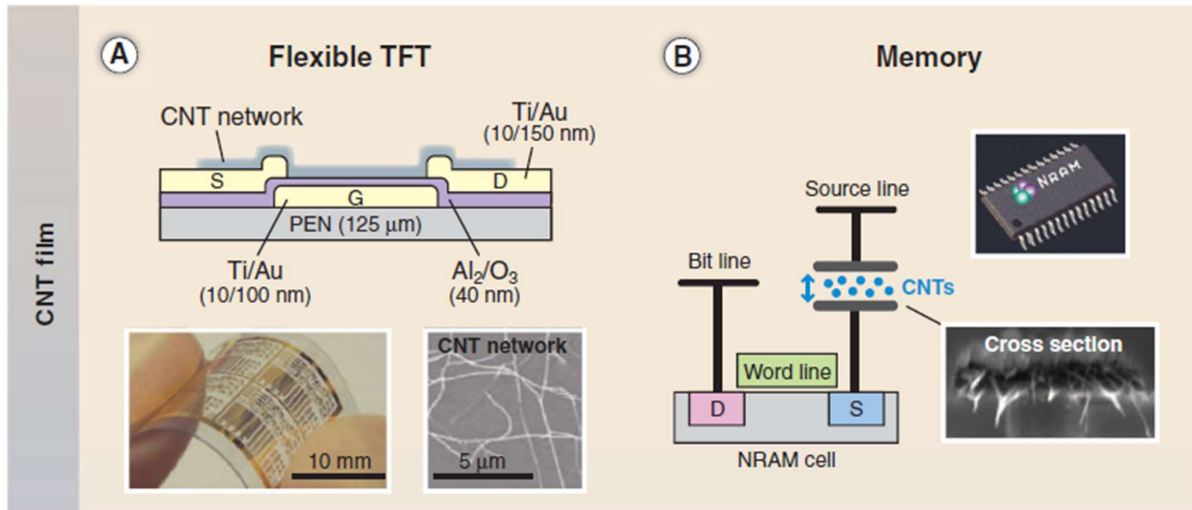


**Figure 8.** CNTs applications in microelectronic devices

### 2.4.3 ENERGY STORAGE

MWCNTs are widely used in lithium ion batteries for notebook computers and mobile phones. In these batteries, small amounts of MWCNTs are blended with active materials and a polymer binder, such as 1 wt% CNT loading in LiCoO<sub>2</sub> cathodes and graphite anodes [33]. Several recent studies showed that CNTs provide increased electrical connectivity, which enhances rate capability and cycle life [34] [35]. In addition, a lot of publications report gravimetric energy storage and power densities for unpackaged batteries and supercapacitors, where normalization is with respect to the weight of active electrode materials. In one of the few recent studies for packaged cells, remarkable performance has been obtained for supercapacitors deploying forest-grown SWCNTs that are binder and additive free; despite the good energy density (16 Wh Kg<sup>-1</sup>) and power density (10 kW kg<sup>-1</sup>), the present cost of SWCNTs is the major downside for their commercialization in this field [30]. Regarding fuel cells, the use of Carbon Nanotubes as a catalyst support can potentially reduce Pt usage by 60% compared with carbon black, and doped CNTs may enable fuel cells that do not require Pt as a catalyst, drastically reducing costs. For organic solar cells, ongoing efforts are exploiting the properties of Carbon Nanotubes to reduce undesired carrier recombination and enhance resistance to photooxidation. However, photovoltaic technologies may incorporate CNT-Si heterojunctions and exploit efficient multiple-exciton generation at p-n junctions formed within individual CNTs [36]. Another good application domain

of carbon nanotube is water purification. Here, tangled CNTs sheets can provide mechanically and electrochemically robust networks with controlled nanoscale porosity. These have been used to electrochemically oxidize organic contaminants, bacteria and viruses [37]. Moreover, membranes using aligned encapsulated CNTs with open ends permit flow through the cave part of nanotubes, enabling low flow resistance for both gases and liquids. This enhanced permeability may enable lower energy costs for water desalination by reverse osmosis in comparison to commercial polycarbonate membranes [38].

#### **2.4.4 BIOTECHNOLOGY**

The last application field of interest for CNTs is the biotechnology. Ongoing interest in Carbon Nanotubes as components of biosensors and medical devices is motivated by the dimensional and chemical compatibility between nanotubes and biomolecules, such as DNA and proteins. At the same time, SWCNT biosensors can exhibit large changes in electrical impedance and optical properties [39] in response to the surrounding environment, which is typically modulated by adsorption of a target on the nanotube surface. The potential toxicity of CNTs remains a concern, although it is emerging that their geometry and surface chemistry strongly influence biocompatibility, and therefore CNT biocompatibility may be engineerable [40].

A final consideration is that organized CNT materials such as forests and yarns are beginning to bridge the gap between the nanoscale properties of CNTs and the length scales of bulk engineering materials. However, understanding is needed of why the properties of carbon nanotubes yarns and sheets, like thermal conductivity and mechanical strength, remain far lower than the properties of individual CNTs. Vice versa, individual CNTs having desired structure with lithographic precision over large substrates would be a breakthrough for electronic devices and scanning probe tips [41].

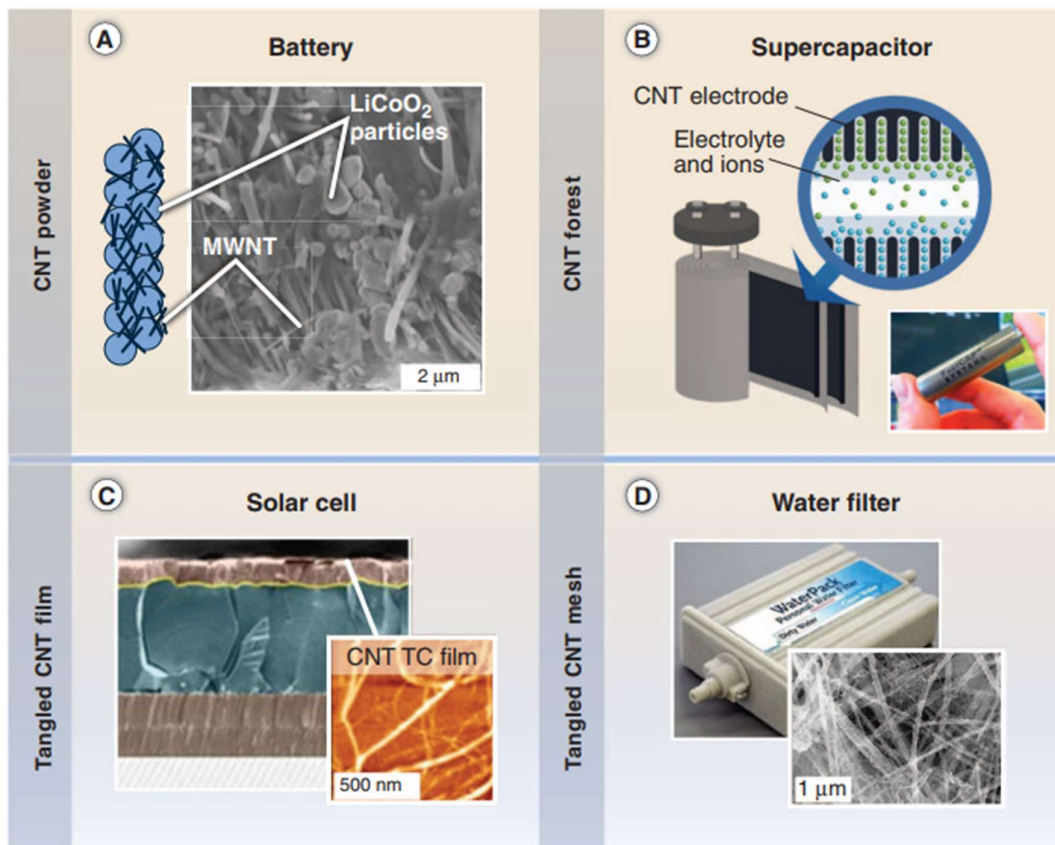


**Figure 9.** Main applications of CNTs in Energy storage (batteries and solar cells)

### 3. CEMENT

#### 3.1 PRODUCTION OF PORTLAND CEMENT

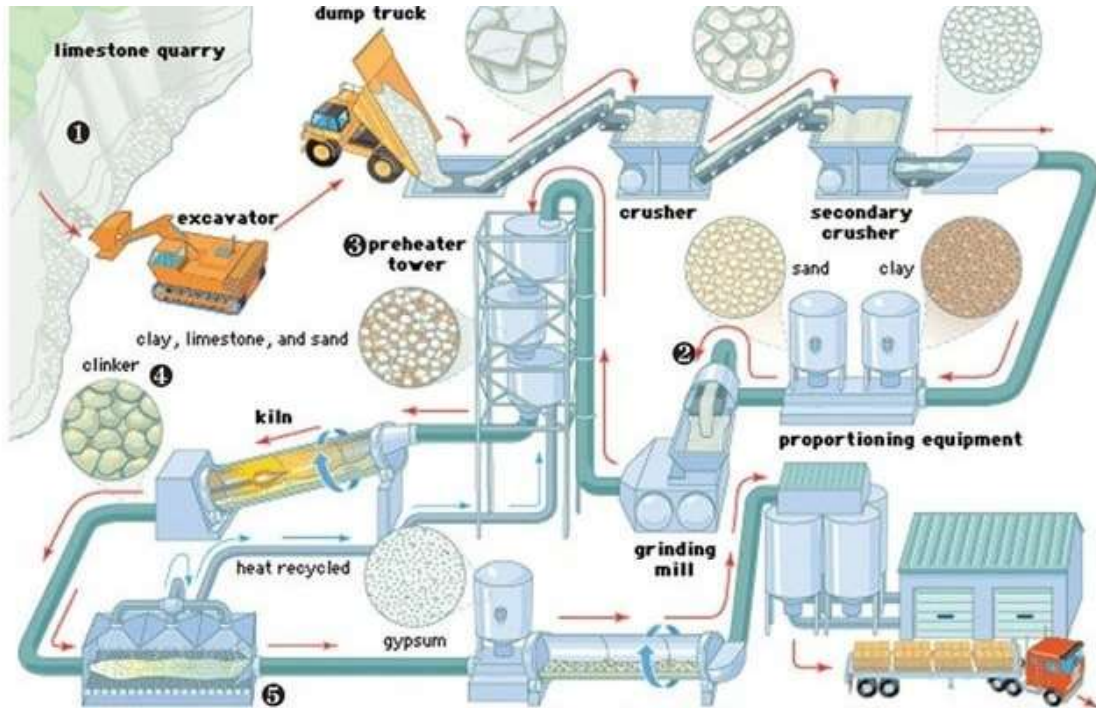


*Figure 10. Full process of the production of Portland cement from limestone quarry to grinding*

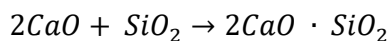
Portland cement is a mixture of tricalcium silicate, dicalcium silicate, tricalcium aluminate, tetracalcium aluminoferrite and gypsum. More than 30 raw materials are known to be used in the manufacture of Portland cement. When water is added, the cement paste hardens and develops binding property as consequence of numerous hydration reactions. These materials are chemically combined through processes of pyrolysis and subjected to subsequent mechanical processing operations to form the final product. The cement manufacture involves four different stages: quarrying, raw material preparation, clinkering and cement preparation [42]. Figure 10 schematically represents the production line of the cement step by step, until the storage of the Portland cement is complete. The process starts with the extraction of the raw material. The composition of the raw material consists of a mixture of about 80% of limestone, which is mainly

composed of  $\text{CaCO}_3$  [43], and 20% of clay or shale, silica, alumina and  $\text{Fe}_2\text{O}_3$ . After the extraction of the raw materials, they are crushed in a quarry which is usually located in the proximity of the cement works. This process is always followed by the raw material preparation which includes a variety of blending and sizing operations to provide a feed with appropriate chemical and physical properties. There are 2 different types of steps regarding the raw material processing, dry or wet. In the case of dry process, limestone and clay are crushed separately and then fed together into a mill. The wet process, instead, consists of the mixing of clay (which is first worked into a paste inside a wash mill, which is a tank used for the grinding of the clay in presence of water) and later crushed lime is added in the end in order to perform the raw material processing. Anyway, in both cases, a laboratory analysis is required to ensure, and eventually adjust, the correct amount of all elements. Then, the finely ground material passes through another process called “clinkering” in which it is dried, heated and then cooled down again. This process transforms the raw material into clinkers, which are grey, glass-hard, spherically shaped nodulus that range from 5 to 25 mm in diameter [44]. The chemical reactions and physical processes can be viewed as follow [43]:

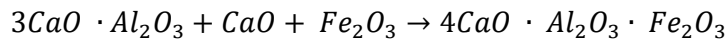
- Evaporation of not combined-water from raw materials (20 – 100°C);
- Dehydration (100 – 430°C) which consists in the formation of silicon, aluminum and iron;
- Calcination (800 – 1000°C) in which it takes place the formation of  $\text{CaO}$ , according with the following reaction:



- Exothermic reactions (1100 – 1300°C): formation of secondary silicate phases:



- Sintering and reactions within the melt (1300 – 1450°C): formation of ternary silicates and tetracalcium aluminoferrates:



- Quenching and crystallization of the various mineral phases

In order to obtain the final product, the clinker is mixed with gypsum and ground. Grinding is a high-cost operation which consumes almost 60% of the total electrical energy involved in a typical cement plant. The electrical energy consumed in the conventional cement making process is in the order of 110 kWh/ton. Of that, about 30% is used for raw materials preparation, while another 40% is used for the final grinding. Finished cement is pumped pneumatically to storage silos from which it is drawn for packing in paper bags or for dispatch in bulk containers and tanks [44].

One of the main downsides of the massive use of the concrete, in which Portland cement is the main glue, in the building industry, is the fact that it has a significant impact on the environment. The production of each ton of Portland cement requires about 1.6 tons of raw materials, primarily quartz and limestone, and releases about 0.8 tons of CO<sub>2</sub> into the atmosphere, thus being responsible for probably 5-7% of the world's greenhouse gas emissions. One of the key challenges for the cement industry is to reduce the greenhouse gas emissions, energy consumption, and natural resources associated with cement production by developing innovative and sustainable cement-based materials.

### 3.2 HYDRATION PROCESS OF PORTLAND CEMENT

Hydration consists of a reaction of an anhydrous compound with water, yielding a hydrated compound. In cement chemistry, hydration refers to the reaction of a non-hydrated cement with water, having chemical and mechanical changes as consequences [45]. Cement hydration involves a collection of coupled chemical processes, each of which occurs at a rate that is determined both by the nature of the process and by the state of the system at that instant. These processes are:

- *Dissolution/dissociation*: This process involves detachment of molecular units from the surface of a solid in contact with water [46].
- *Diffusion*: describes the transport of solution component through the pore volume of cement past or along the surface of solids on the adsorption layer [47].

- *Growth*: involves surface attachment, the incorporation of molecular units into the structure of a crystalline or amorphous solid within its self-adsorption layer [48].
- *Nucleation*: initiates the precipitation of solids heterogeneously on solid surfaces or homogeneously in solution, when the bulk free energy driving force for forming the solid overweighs the energetic penalty of forming the new solid-liquid interface [49].
- *Complexation*: these are reactions between ions to form adsorbed molecular complexes on solid surfaces.
- *Adsorption*: accumulation of ions or other molecular units at an interface, such as the surface of a solid particle in a liquid.

These processes may operate in series, in parallel, or in some more complex combination. For example, even simple crystal growth from solution involves diffusion of solute to the proximity of an existing solid surface, adsorption of the solute onto the surface, complexation of several solute species into a molecular unit that can be incorporated into the crystal structure and, finally, attachment and equilibration of that molecular unit into the structure [50].

The chemical composition of cement clinker is usually expressed as weight percentage of oxides. The most important oxides in Portland cement clinkers are CaO, SiO<sub>2</sub>, MgO, Al<sub>2</sub>O<sub>3</sub> and Fe<sub>2</sub>O<sub>3</sub>. The oxides occur in the cement clinker structure in forms of different clinker minerals [51]. For simplicity, and according to the conventional cement chemistry notation as the Bogue formula, the oxides previously cited can be denoted as C (CaO), A (Al<sub>2</sub>O<sub>3</sub>), F (Fe<sub>2</sub>O<sub>3</sub>), S (SiO<sub>2</sub>) and M (MgO).

Component	SiO <sub>2</sub>	Al <sub>2</sub> O <sub>3</sub>	Fe <sub>2</sub> O <sub>3</sub>	CaO	MgO	SO <sub>3</sub>
weight (%)	21.9	6.9	3.9	63.0	2.5	1.7

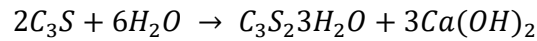
**Figure 11.** Chemical composition of Portland cement clinker

### C<sub>3</sub>S

The main component of the Portland cement is tricalcium silicate (C<sub>3</sub>S), also called Alite. It controls in large extent the cement strength and hardening [52]. Historically, the overall process of hydration was divided into four or five stages, defined by somewhat arbitrary points on a plot of hydration rate vs time, as shown in Figure 8. The names of the processes taking place during the

hydration of cement are: (1) Initial reaction, (2) period of slow reaction, (3) acceleration period, (4) deceleration period [53].

The Initial period (1) is characterized by rapid reactions between  $C_3S$  and water that begin immediately upon wetting, characterized by a large exothermic signal in isothermal calorimetry experiments [54]. The heat released by wetting in cement powder contributes to this early exothermic signal, but significant heat is also released by dissolution of  $C_3S$ . The enthalpy of congruent  $C_3S$  dissolution is  $-138 \text{ kJ mol}^{-1}$ , based on the reaction:



Chemical analyses of the solution phases have showed evidence that  $C_3S$  dissolves congruently and quite rapidly in the first seconds after wetting.

The slow dissolution of  $C_3S$  (2) would continue to be rapid up to much higher solution concentration of calcium and silicates if not for the formation of the passivating hydrate layer. It presents a monoclinic structure and it constitutes about 50% to 70% of Portland cement by mass. Alite tends to dominate the early hydration period that comprises setting and early strength development because it is the component most responsible for formation of the calcium silicate hydrate gel (C-S-H), that is the principle product of hydration.

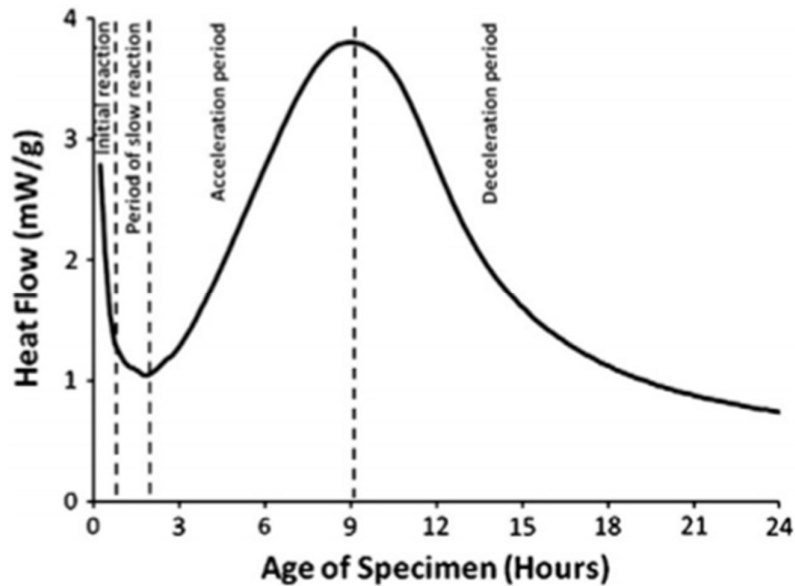


**Figure 11.** Rate of Alite ( $C_3S$ ) hydration as a function of time given by isothermal calorimetry measurement

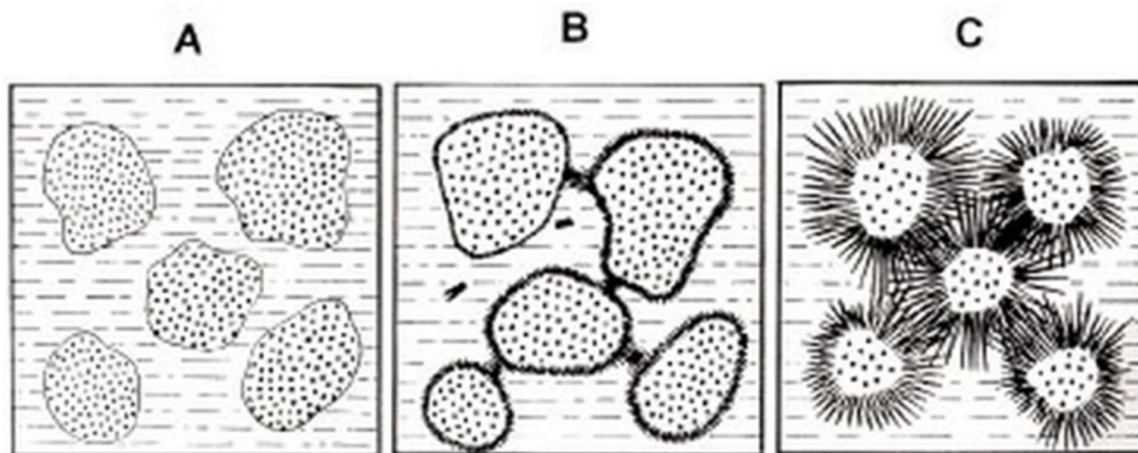
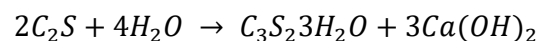


**Figure 12.** Schematic representation of  $C_3S$  hydration

### $C_2S$

The second protagonist of the reaction of hydration is  $C_2S$ . The reaction that involves  $C_2S$  (also called Belite) is:



In this case, as before, it is possible to distinguish different stages of reactions. An extended induction period, with a very low rate of hydration, is followed by a second stage of gradual increase of the hydration rate, since it slows down again in the third period of the hydration [55].

### $C_3A$

$C_3A$  plays a crucial role in the hydration and durability of Portland cement, even though the content of this phase is only about 5-10% by mass of the Portland cement. On one hand, the initial reaction period (called induction period) and the shoulder peak in Portland cement hydration are

related to the  $C_3A$  hydration kinetics [56], and thus the hydration of  $C_3A$  impacts the early age properties of the cement pastes and concrete such as setting time, workability, etc. On the other hand, numerous researches report that  $C_3A$  interacts strongly with supplementary cement materials and chemical admixtures [57] [58], which further determines the performance of  $C_3A$  in concrete.

Some researchers have focused on the hydration of  $C_3A$  in the absence of gypsum. Platelets of calcium aluminate hydrates, such as  $C_2AH_8$ ,  $C_4AH_{13}$ ,  $C_4AH_{19}$  etc., precipitate immediately when  $C_3A$  reacts with water alone due to the high hydraulic activity of  $C_3A$  [59]. The metastable phases ( $C_2AH_8$ ,  $C_4AH_{13}$ ,  $C_4AH_{19}$  etc.) then convert to thermodynamically stable phase hydrogarnet ( $C_3AH_6$ ) at later age [60] [61].

Flash set will occur in Portland cement hydration without gypsum, therefore, proper dosage of gypsum is required to be ground with clinkers in the process of cement production to control the setting time of cement [62]. For our purposes in discussing kinetic mechanisms, we find it helpful to consider the hydration of  $C_3A$  in the presence of gypsum into three periods indicated in the calorimetry plot of hydration rate versus time shown in Figure 10: (1) initial reaction, (2) period of slow reaction, called induction period, (3) renewed hydration of  $C_3A$ . In the initial period,  $C_3A$  reacts with gypsum to form ettringite ( $C_6AS_3H_{32}$ ) releasing a large amount of heat. In the subsequent induction period, the reaction slows down significantly, during when the heat released is quite low. The hydration of  $C_3A$  usually does not enter the third period until the exhaustion of solid gypsum in the system. The renewed hydration of  $C_3A$  is featured by a characteristic sharp peak resulted from the reaction between  $C_3A$  and ettringite leading to the formation of monosulphoaluminate (s-AFm). There are two prevailing mechanisms to describe the hydration kinetics of the third period. One is the dissolution-controlled mechanism proposed by Minard [63] and the other supported by Quennoz [64] [65] is related to the nucleation and growth of s-AFm.

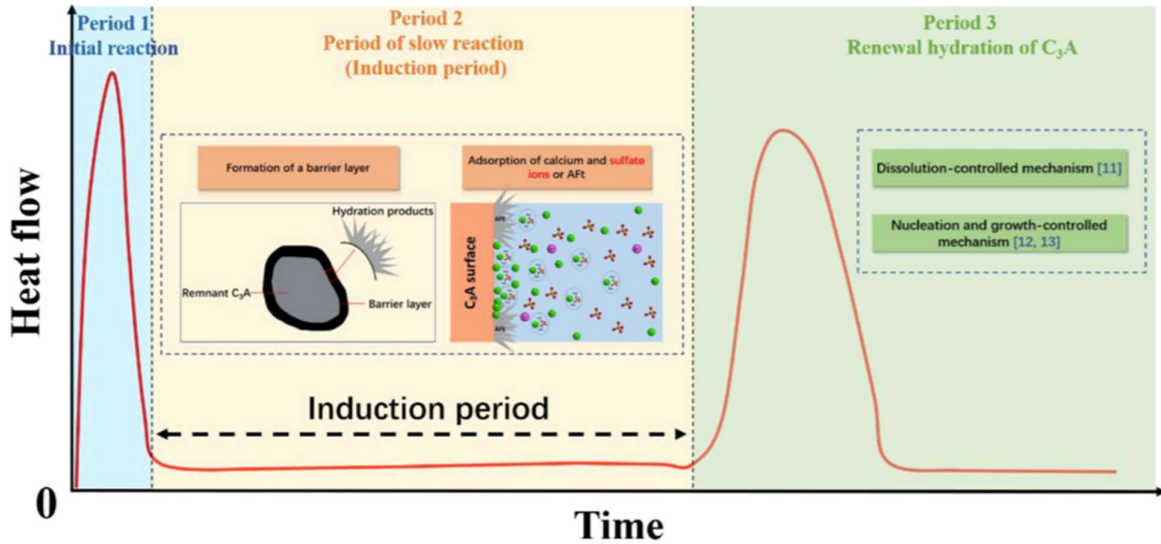


**Figure 13.** Idealized hydration rate of C3A in the presence of gypsum as a function of time

#### C<sub>4</sub>AF

Unlike the other three phases (C<sub>3</sub>S, C<sub>2</sub>S and C<sub>3</sub>A), the tetracalcium aluminoferrite phase (C<sub>4</sub>AF), also known as Brownmillerite, is the only variable phase with unfixed composition in ordinary Portland cement. Brownmillerite is also an important component in the calcium alluminate cements and calcium sulfoaluminate cements. Due to its excellent mechanical and durability properties, this phase attracts extensive attentions and has been deeply studied.

When Brownmillerite is in contact with water, metastable C-(A,F)-H hydrates (hydroxy-AFm) are rapidly formed on the surface of the anhydrated grains and eventually converted to a stable hydrogarnet phase C<sub>3</sub>(A,F)H<sub>6</sub>. Whether Fe could be a substitute for Al in the structure of these hydration products (C-(A,F)-H, C<sub>3</sub>(A,F)H<sub>6</sub>) is still debatable, but it is generally recognized that the Al/Fe ratio of the original C<sub>4</sub>AF is much less than in the crystalline hydration products [66]. It has been reported that the detection of an amorphous iron-rich gel or iron hydroxide (FH<sub>3</sub>) in the hydrates could explain the high Al/Fe ratio in the crystalline hydration products [67].

In the presence of gypsum, the primary hydrates (C-(A,F)-H) are substituted by ettringite (AFt) which is deemed to intensely retard the hydration of C<sub>4</sub>AF. Three prevalent theories have been proposed on the retardation mechanism of this process. (a) The generation of a dense and coherent ettringite layer envelops the anhydrous C<sub>4</sub>AF, and thus hinders further hydration. (b)

Retardation is due to adsorption of sulfate ions on  $C_4AF$ . (c) The formation of a C-(A,F)-gel acts as a nucleation “agent” for ettringite precipitation from solution.

### 3.3 EFFECT OF CNTS ON CEMENTITIOUS COMPOSITE HYDRATION AND FLOWABILITY

Carbon Nanotubes are chemically inert materials, but it can promote the pozzolanic reaction of cementitious materials, mainly during the early age hydration. CNT within the cement composite can act as a nucleation agent and promote the sedimentation and growth of hydration products. Preferably, calcium silicate hydrate (C-S-H) gel should be observed around the CNTs within the cement composites. Several studies were carried out to investigate the influence of CNTs on the hydration of cementitious composites.

Makar investigated the influence of SWCNTs on the hydration of cement paste [68]. In his study, cement paste combining OPC (ordinary Portland cement) and cement paste without carbon nanotubes were sonicated for 2 h, and then an isothermal conduction calorimetry test was conducted. OPC with CNTs showed a higher heat of hydration initially and after 6 h of hydration than the sonicated paste without CNTs. The composite sample with nanotubes showed a higher level of initial surface activity than the sonicated OPC.

The development of the maximum heat flow peak of the composite sample containing CNTs was accelerated. Besides, the derivative heat flow of the composite paste significantly increased. The acceleration in the development of the maximum heat flow peak and a higher derivative heat flow peak indicates the acceleration in the hydration of the composite material. Sonicated OPC with CNTs produced much more initial heat than sonicated OPC but less coverage of exposed OPC surface by tricalcium aluminate ( $C_3A$ ) hydration products. The carbon nanotube is a chemically inert material, and the acceleration in hydration may be attributed to the nucleation effects. SEM results also indicate the preferential presence of C-S-H around the nanotubes, which supports the concept of carbon nanotubes as a nucleation agent. The heat flow measured by the isothermal conduction calorimetry test of the composite samples is shown in Figure 14.

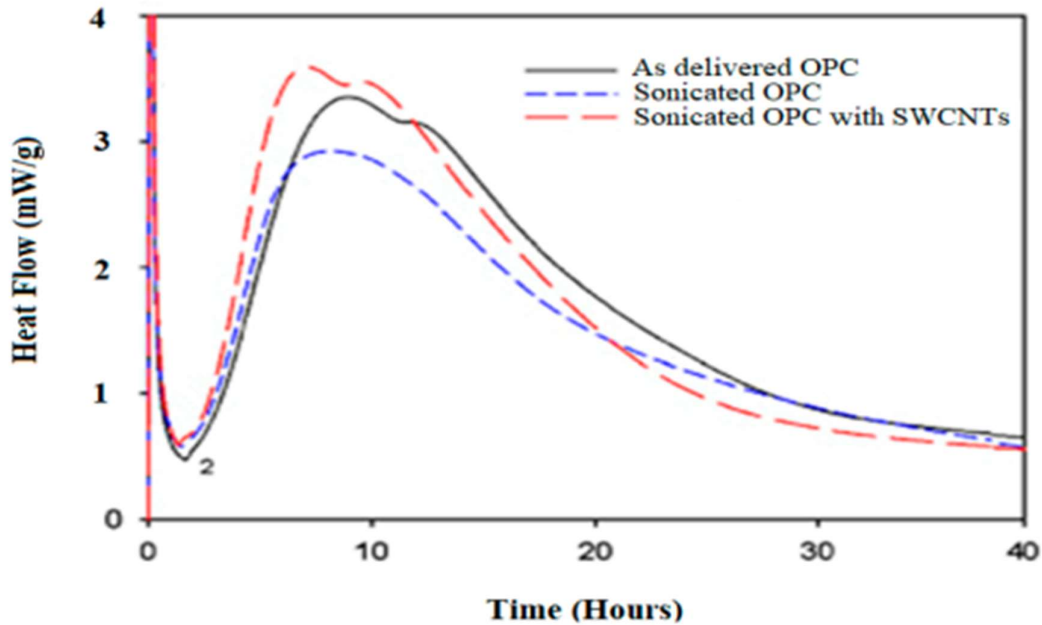


**Figure 14.** Heat flow measured by isothermal conduction calorimetry

Other studies showed that the incorporation of CNTs into the cement paste had a positive influence on the exothermic rate. The acceleration in hydration and a higher produced heat were identified in the samples containing CNTs compared to the control sample without CNTs. This evidence was explained by the fact that the addition of nanotubes to the cement particles provided reaction sites for the hydration reaction mechanism, which resulted in calcium ions hydrolyzed and absorbed in high concentrations, speeding up the hydration reaction [69]. Moreover, when CNTs are incorporated into the cement paste, the heat flow curves shifted to shorten hydration times and enlarge the heat flow peak. The shorter hydration time of CNTs embedding cement paste indicates the acceleration of the hydration reaction mechanism, which can be attributed to the enhanced dispersion of cement paste by nucleation sites [70].

Flowability, or workability, is one of the important factors in concrete mix design. Several factors, like the fineness of the cement powder, cement content, increased ratio of coarse and fine aggregates, water/cement ratio and the use of chemical admixtures, usually influence the

flowability of conventional concrete. The incorporation of CNTs into cementitious composites increases the viscosity and reduces the flowability of the composite [71].

### EFFECT OF NANOPARTICLES ON CEMENT COMPOSITES

Nanoparticles exert beneficial influence on the properties and performance of cement through various mechanisms including densification of microstructure. Nanoparticles of pozzolanic materials, viz. nano silica, react at very early ages with  $\text{Ca}(\text{OH})_2$  resulting in formation of additional calcium silicate hydrate (C-S-H) through pozzolanic reaction. Carbon nanotubes are another type of nanoparticles which act as reinforcement for cementitious matrices improving their flexural strengths, fracture toughness and other engineering properties. Such improvements in cement performance through use of nanoparticles could result in lower clinker content in concrete without compromising on strength and other properties. This in turn could be expected to lead to greater sustainability and conservation of resources. In addition, these nano additions give special properties to concrete.

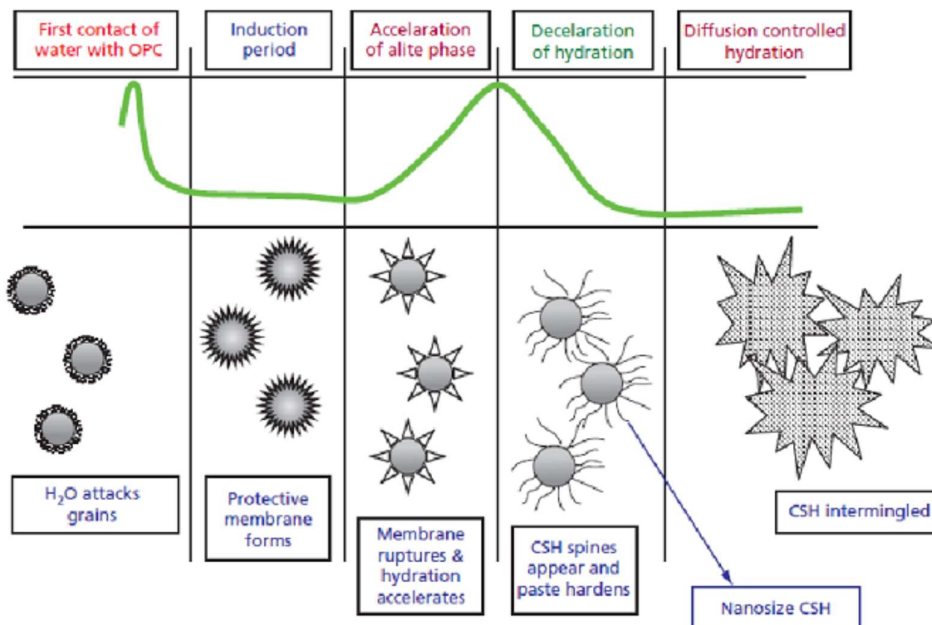


**Figure 15.** Role of nano-additives in cement hydration process

Nanosilica in cementitious systems improves various properties such as strength, hydration, durability, etc. Micro and nano-scaled silica particles have a filler effect by filling up the voids between the cement grains. Beside physical effect as obtained by addition, nanosilica has a pozzolanic reactivity which is much higher compared to silica fume. Both the effects are very important in developing ultra-high-performance concrete. There may be two possible reaction mechanisms during the hydration of cement in presence of nanosilica. When nanosilica is added to cement grains,  $\text{H}_2\text{SiO}_2$  forms and reacts with the available  $\text{Ca}^{2+}$  ions which forms an additional calcium–silicate–hydrate (C–S–H) and these C–S–H particles are spread in the water between the cement particles and serve as seeds for the formation of more compact C–S–H phase. The overall reaction is the one given below in Figure 16.

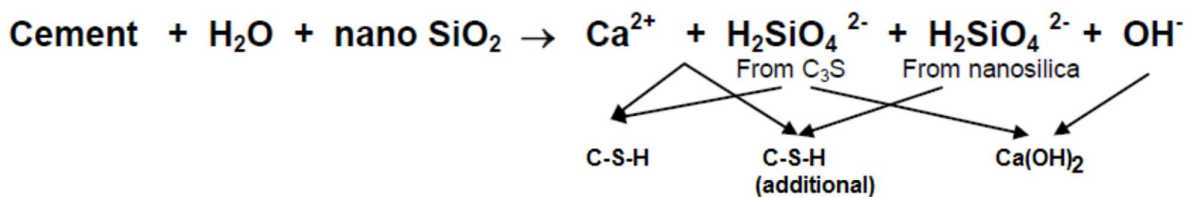


**Figure 16.** Overall cement hydration reaction with the presence of nanosilica

## CONCRETE AND CARBON-BASED MATERIALS

Concrete is the most widely used construction material. As structural materials, cementitious materials are almost brittle and susceptible to cracking and have no functional properties. Nanotechnology is introduced into cementitious materials to address these issues. Nano materials, especially nano carbon materials (NCMs) were found to be able to improve/modify the mechanical properties, durability and functional properties of cementitious materials due to their excellent intrinsic properties and composite effects [72]. Carbon nanotubes have many advantageous mechanical and electrical properties such as high strength, high conductivity and, therefore, are attractive for producing fiber-reinforced concrete. The incorporation of fibers at the nanoscale allows the control of the matrix cracks at the nanoscale level [73]. Mechanically, CNTs show elastic behavior, with a Young's Modulus of approximately 1 TPa and a density of about  $1.33 \text{ g/cm}^3$ . Single walled CNTs have yield stresses between 20 and 60 GPa, with measured yield strains of up to 10%. Moreover, carbon nanotubes can bear torsion and bending without breaking. Since CNTs exhibit great mechanical properties along with extremely high aspect ratios (length-to-diameter

ratio) ranging from 30 to more than many thousands, they are expected to produce significantly stronger and tougher cement composites than traditional reinforcing materials (e.g. glass fibers or carbon fibers). In fact, because of their size (ranging from 1 nm to tens of nm) and aspect ratios, CNTs can be distributed in a much finer scale than common fibers, giving as a result a more efficient crack bridging at the very preliminary stage of crack propagation within composites [74]. However, the major challenge associated with the incorporation of CNTs in cement-based materials is the problem of poor dispersion [75]. Poor dispersion of nanotubes leads to the formation of many defect sites in the nanocomposite and limits the efficiency of CNTs in the matrix [76].

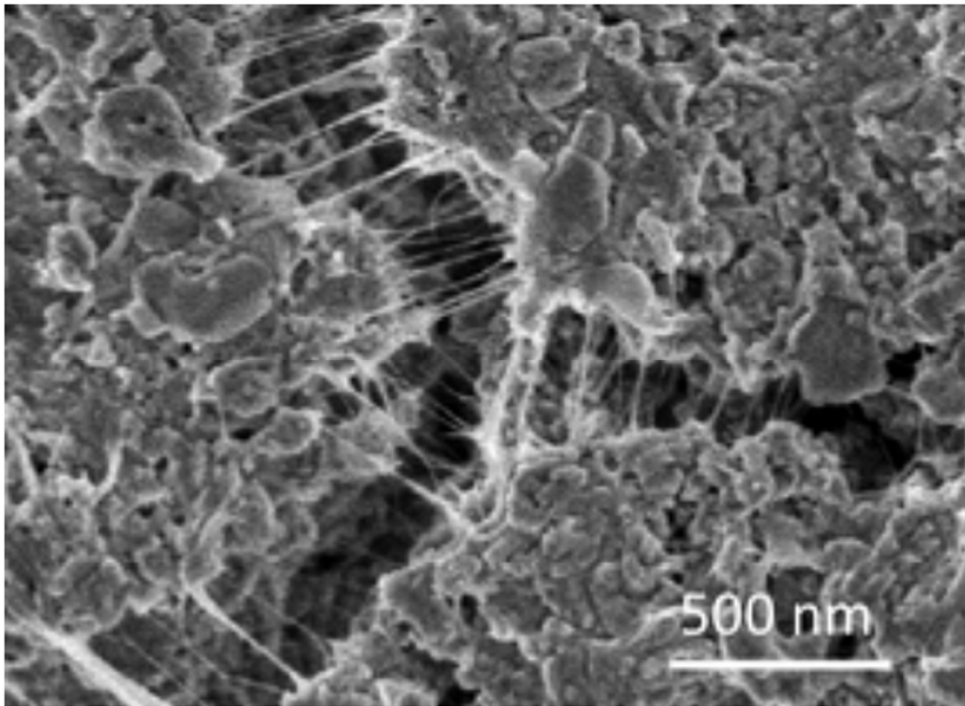


**Figure 17.** Crack-bridging effect in cement CNTs composites [4A]

#### **4. FUNCTIONALIZATION OF CARBON NANOTUBES**

The full potential of nanotubes as reinforcements has been severely limited due to poor interfacial interaction, (Van der Waals) between CNTs and cement matrix. The nature of dispersion problem for CNTs is rather different from other conventional fillers, such as spherical particles and carbon fibers, because CNTs are characteristic of small diameter in nanometer scale with high aspect ratio (>1000) and thus possessing large surface area. In addition, the commercialized CNTs are supplied in the form of heavily entangled bundles, resulting in inherent difficulties in dispersion.

These approaches can be simply divided into chemical (covalent) and physical (noncovalent) functionalization as interactions between active materials and CNTs.

#### **4.1 NON-COVALENT FUNCTIONALIZATION**

The non-covalent functionalization is an alternative method for tuning the interfacial properties of nanotubes. The CNTs are functionalized non-covalently by aromatic compounds, surfactants, and polymers, employing  $\pi$ - $\pi$  stacking or hydrophobic interactions for the most part. In these approaches, the non-covalent modifications of CNTs can do much to preserve their desired properties, while improving their solubilities quite remarkably. It will summarize as followed: aromatic small molecule absorption, polymer wrapping, surfactants, biopolymers and endohedral method. Aromatic molecules, such as pyrene, porphyrin, and their derivatives, can and do interact with the sidewalls of CNTs by means of  $\pi$ - $\pi$  stacking interactions, thus opening up the way for the non-covalent functionalization of CNT [77].

#### **4.2 COVALENT FUNCTIONALIZATION**

The end caps of nanotubes tend to be composed of highly curved fullerene-like hemispheres, which are therefore highly reactive, as compared with the side walls. The sidewalls themselves contain defect sites such as pentagon- heptagon pairs called Stone-Walls defects,  $sp^3$ -hybrideized defects, and vacancies in the nanotube lattice [78].

Chemical functionalization is based on the covalent bond of functional groups onto carbon form of CNTs. It can be performed at the end caps of nanotubes or at their sidewalls which have many defects. Direct covalent sidewall functionalization is associated with a change of hybridization from  $sp^2$  to  $sp^3$  and a simultaneous loss of p-conjugation system on graphene layer. This process can be made by reaction with some molecules of a high chemical reactivity. In the first approach, fluorination of CNTs has become popular for initial investigation of the covalent functionalization because the CNTs sidewalls are expected to be inert [79].

Another method is chemical functionalization of CNTs. These intrinsic defects are supplemented by oxidative damage to the nanotube framework by strong acids which leave holes functionalized with oxygenated functional groups. In particular, treatment of CNTs with strong acid such as

$\text{HNO}_3$ ,  $\text{H}_2\text{SO}_4$  or a mixture of them, or with strong oxidants such as  $\text{KMnO}_4$ , ozone, reactive plasma tend to create defect on the lattice structure of the tubes thus generating oxygenated functional groups such as carboxylic acid, ketone, alcohol and ester groups. These group can achieve as starting point for grafting several complex chemical groups on the surface of CNTs [80].

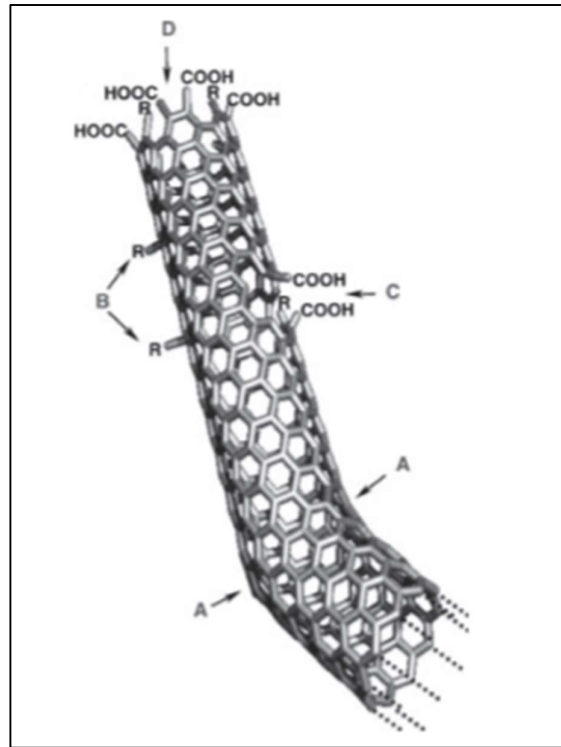


**Figure 18.** Typical defects of a CNT surface after covalent functionalization

## 6. MATERIALS AND METHODS

<b>Chemical analysis (%)</b>	SiO <sub>2</sub>	Al <sub>2</sub> O <sub>3</sub>	Fe <sub>2</sub> O <sub>3</sub>	CaO	SO <sub>3</sub>	MgO	Na <sub>2</sub> O	K <sub>2</sub> O
	22.4	2.96	2.33	66.6	2.13	0.95	0.10	0.15
<b>Bogue composition (%)</b>	C <sub>3</sub> S	C <sub>2</sub> S		C <sub>3</sub> A		C <sub>4</sub> AF		
	65.3	18.6		4.35		7.14		

*Figure 20 - Chemical Composition of Cement 52,5R*

In the previous chapters, a preview of materials for the preparation of carbon nanotubes cement composites was provided. The samples were produced and characterized at the laboratories of the Department of Applied Science and Technology (DISAT) of Politecnico di Torino, while the mechanical tests in order to evaluate the compressive and bending strengths of the samples were performed in the laboratories of the Department of Structural and Geotechnics Engineering (DISEG).

### 6.1 CARBON NANOTUBES CHARACTERIZATION

#### 6.1.1 THERMOGRAVITOMETRIC ANALYSIS (TGA)

Thermogravimetric analysis (TGA) is an analytical technique that measure the weight of a small CNT sample (typically 30-40 mg or less) as a function of time or temperature, hence it gives a quantitative description of the thermal stability of the material and it gives informations about the amount of the corresponding residue of the sample. The measurement is normally carried out in an atmosphere such as Ar/N<sub>2</sub>/He or in air (O<sub>2</sub>), to understand the thermal stability of the materials in an inert atmosphere or to study their thermo-oxidative stability, respectively. TGA experiments can be carried out as either isothermal or non-isothermal (dynamic) weight-loss measurement. The isothermal method requires an almost instantaneous heating of the sample to the desired temperature, followed by maintaining that temperature for a specified time. This method is very

efficient to evaluate the weight loss of polymeric samples. On the other hand, non-isothermal methods require a program with a linear increase in sample temperature with respect to time. TGA instruments usually consists of a high-precision balance with a pan containing the sample and the pan is placed in a small electrically heated furnace containing a thermocouple that accurately measures the temperature. [81]

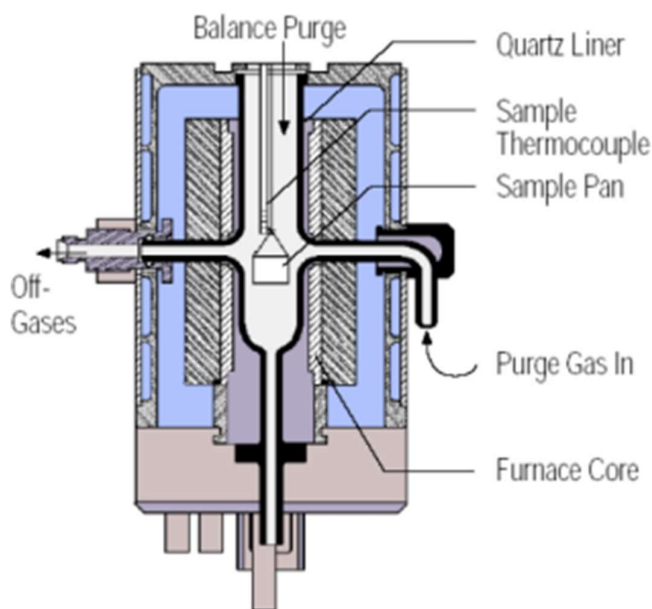


**Figure 22.** Scheme of a generic Thermogravimetric Analysis instrument [3]

Since the instrument records the weight of the sample with respect to time, therefore the instrument needs to have a high degree of precision in measurement such as weight (wt), temperature (T), temperature change ( $\Delta T$ ) and time (t). Once the experiment is over, the data can be presented in terms of percent of weight change related to the absolute temperature or time, which is known as a TGA thermogram. In addition to the TGA thermogram, a derivative weight loss curve known as Differential Thermogravimetric analysis (DTA) can be used to understand a lot of very interesting points of the curve. In fact, from this derivative curve can be evaluated the onset decomposition temperature, the temperature at which the rate of decomposition is at a maximum, end decomposition temperature as well as the number of steps involved in the thermal degradation of the sample. Each step of weight loss corresponds to a peak in the DTA that could be due to one of a series of degradation processes occurring in a specific temperature range.

However, an establishment of a few fixed experimental parameters such as heating rate, initial sample mass or the type of atmosphere of the experiment, must be set.

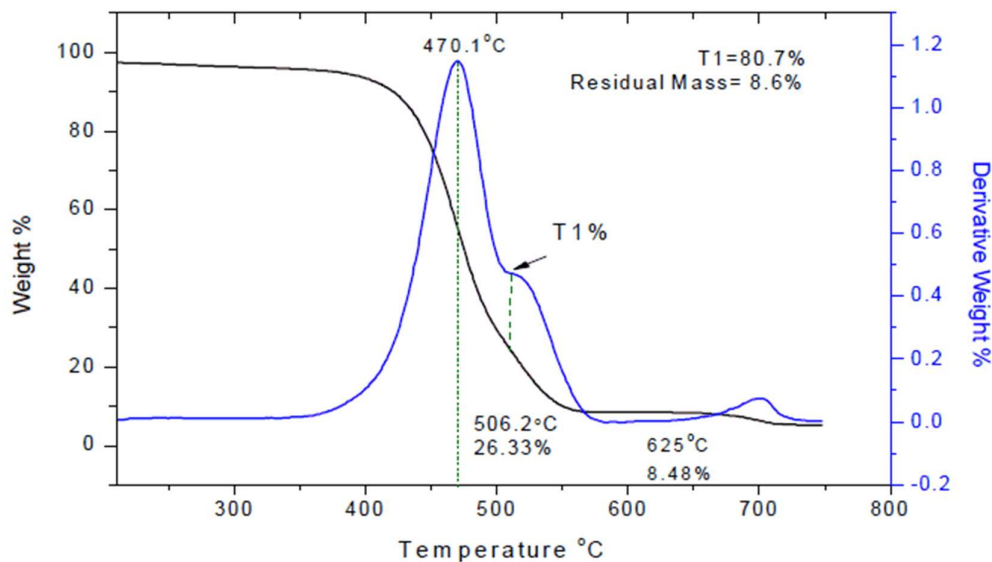


**Figure 23.** Example of TGA curve for pristine Carbon Nanotubes [4]

## 6.1.2 RAMAN SPECTROSCOPY

### 6.1.2.1 THEORY OF RAMAN SPECTROSCOPY

Raman Spectroscopy is a spectroscopic technique typically used to determine vibrational modes of molecules, although rotational and other low-frequency modes of systems may also be observed [82]. The phenomena underlying Raman Spectroscopy can be described with reference to infrared spectroscopy as showed in Figure 5. The primary event in infrared adsorption is the transition of a molecule from a ground state ( $M$ ) to a vibrationally excited state ( $M^*$ ) by absorption of an infrared photon with energy equal to the difference between the energies of the ground and the excited states. The reverse process, called infrared emission, occurs when a molecule in the excited state ( $M^*$ ) emits a photon during the transition to a ground state ( $M$ ). In infrared spectroscopy, one derives information by measuring the frequencies in terms of characteristic vibrational motion of

the molecule. In complex molecules, some of the frequencies are associated with functional groups that have the characteristic localized mode of vibrations.

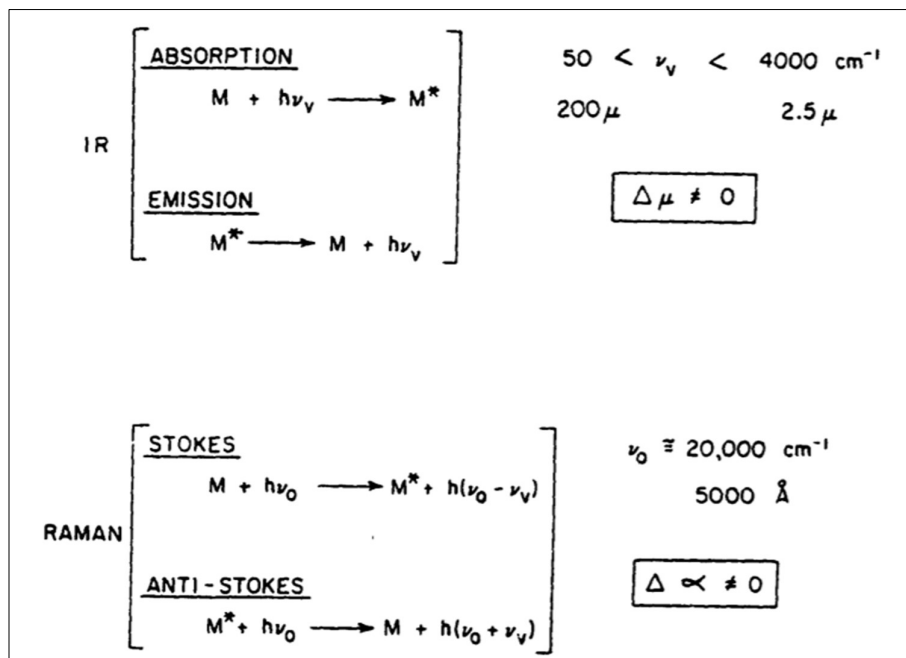


Figure 24. Comparison of IR and Raman spectroscopy phenomena [5]

In the Stokes process, which is the parallel of absorption, the scattered photons are shifted to lower frequencies as the molecules abstract energy from the exciting photons ( $\nu_0 - \nu_v$ ); in the anti-Stokes process, which is the parallel of emission, the scattered photons are shifted to higher frequencies as they pick up the energy released by the molecules in the course of transition to the ground state. In addition, a substantial number of transitions to the ground state. In addition, a substantial number of the scattered photons are not shifted in frequency. The process which gives rise to these photons is known as Rayleigh scattering. This scattering arises from density variations and optical heterogeneities and is many orders of magnitude more intense than Raman scattering [83].

A Raman spectrum is obtained by exposure of a sample to a monochromatic source of exciting photons, and measurement of the light intensity at the frequencies of the scattered light. Because the intensity of the Raman scattered component is much lower than that of the Rayleigh scattered

component, filters and diffraction gratings are used to suppress the latter component. A highly sensitive detector is required to detect weakly scattered Raman photons [84].

In conventional Raman spectroscopy where visible laser radiation is used, the exciting photons are typically of much higher energies than those of the fundamental vibrations of most chemical bonds or systems of bonds, usually by a factor ranging from about 6 for O-H and C-H bonds to about 200 for bonds between very heavy atoms, as for example in I<sub>2</sub>. The 514.5 and 488 nm lines from an argon ion laser are often used as exciting frequencies. In contrast, in the case of FT Raman spectroscopy, excitation with a laser is usually carried out in the near-IR region (1064 nm). The energies of the exciting photons are higher by factors that are one-half or less of the above-mentioned values. Another point to consider in near-IR excited Raman is that, for some samples, absorption of Raman scattered photons due to overtone and combination modes of molecular vibrations can occur.

#### **6.1.2.2 CONVENTIONAL RAMAN INSTRUMENT**

Several stages are involved in the acquisition of a Raman spectrum using a conventional approach. A sample is mounted in the sample chamber and laser light is focused on it with the help of a lens. Generally, liquids and solids are sampled in a Pyrex capillary tube. Solids are sampled either as pellets or are examined directly without any sample preparation. The scattered light is collected using another lens and is focused at the entrance slit of the monochromator. Monochromator slit widths are set for the desired spectral resolution. The monochromator effectively rejects Rayleigh scattering and stray light and serves as a dispersing element for the incoming radiation; sometimes more than one monochromator is used to obtain high resolution and/or better suppression of the Rayleigh line. The light leaving the exit slit of the monochromator is collected and focused on the surface of a detector. This optical signal is converted to an electrical signal within the detector and further manipulated using detector electronics. In a conventional Raman system using a photomultiplier tube (PMT) detector, the light intensity at various frequencies is measured by scanning the monochromator. In contrast, when a multichannel detector is used a spectral range is simultaneously recorded [85].

A typical conventional Raman system consists of the following basic components: an exaltation source, usually a visible-light laser, optics for sample illumination and collection of sample-scattered light, a monochromator and a signal processing system consisting of a detector and a data processing unit. A diagram showing the various components of a Raman spectrometer is shown in Figure 6.

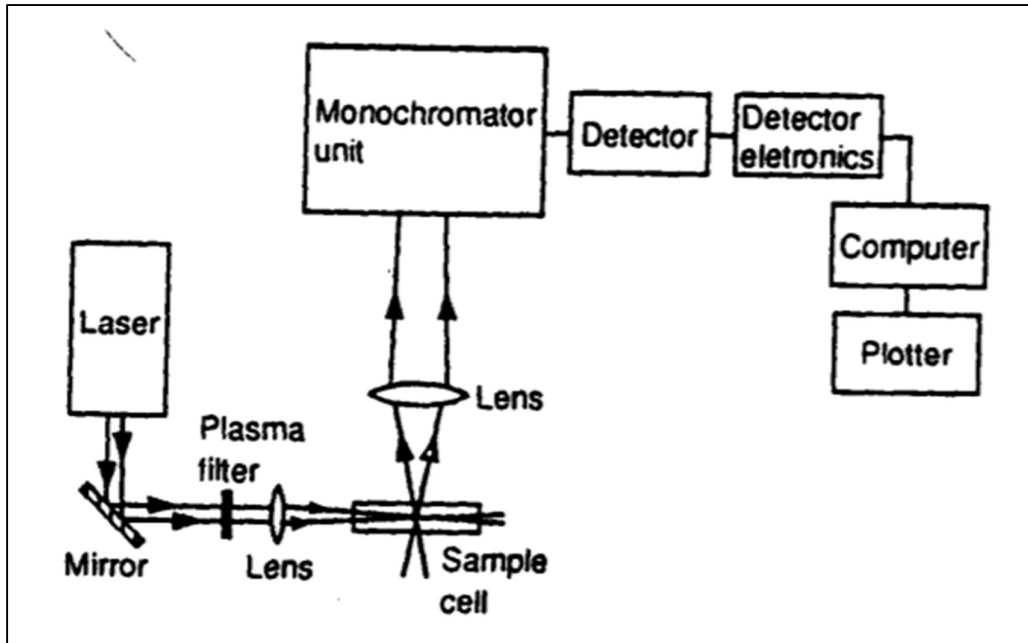


Figure 25. Scheme of a conventional Raman instrument [84]

## 6.2 CARBON NANOTUBES FUNCTIONALIZATION

For the process of functionalization of CNT surface, a chemical (also called covalent) functionalization has been used. As previously discussed in the CNTs functionalization chapter, the covalent functionalization consists of damaging the nanotube framework by using strong acids which leaves holes in which -COOH groups are bonded by the reaction with the acid.

Those type of oxygenated functional groups will be able to drastically improve the dispersion in water solution and also, they will promote the surface interaction with the cement matrix in the concrete composite.

The acid chosen for the functionalization of the carbon nanotubes was the sulfonitric mixed acid, which is a mixture of 3 parts of sulfuric acid ( $H_2SO_4$ ), and 1 part of nitric acid ( $HNO_3$ ): 1  $HNO_3$ : 3  $H_2SO_4$ .

Also, in order to see the possible effects of the time of functionalization of the carbon nanotubes, and eventually achieve a better interaction between the reinforcement and the cement matrix, several sonication times were performed. The time interval between every sonication process that has been chosen was 15 minutes. So, the several preparations of functionalized CNTs are:

- CNTs + 1  $HNO_3$  : 3  $H_2SO_4$  sonicated for 15 minutes.
- CNTs + 1  $HNO_3$  : 3  $H_2SO_4$  sonicated for 30 minutes.
- CNTs + 1  $HNO_3$  : 3  $H_2SO_4$  sonicated for 45 minutes.
- CNTs + 1  $HNO_3$  : 3  $H_2SO_4$  sonicated for 60 minutes.
- CNTs + 1  $HNO_3$  : 3  $H_2SO_4$  sonicated for 75 minutes.
- CNTs + 1  $HNO_3$  : 3  $H_2SO_4$  sonicated for 90 minutes.

Sample N°	Time [min]	Temperature [°C]	Acid	Dispersant
1	15	30	1 $HNO_3$ : 3 $H_2SO_4$	No
2	30	30	1 $HNO_3$ : 3 $H_2SO_4$	No
3	45	30	1 $HNO_3$ : 3 $H_2SO_4$	No
4	60	30	1 $HNO_3$ : 3 $H_2SO_4$	No
5	75	30	1 $HNO_3$ : 3 $H_2SO_4$	No
6	90	30	1 $HNO_3$ : 3 $H_2SO_4$	No

**Figure 26.** Table showing the different functionalization times for the 6 CNTs samples in the 1  $HNO_3$  : 3  $H_2SO_4$  acidic solution

Here, the method used for the functionalization of the carbon nanotubes is described.

The first thing that needs to be done is to take the right amount of carbon nanotubes needed to make at least 4 samples of cement-CNT composites. It has been decided to use 0,5g of pristine CNTs which were weighed by a scientific weighing scale "Radwag" from "SAVATEC Strumenti". After weighing the amount of carbon nanotubes needed for the functionalization, the next step consists of preparing the acids mixture.

The two acids needed for the mixture were  $\text{HNO}_3$  (nitric acid given by "Carlo Erba reagents") and  $\text{H}_2\text{SO}_4$  (sulfuric acid given by "SIGMA-ALDRICH"). Both acids were poured into a becker respectively. In order to make the sulfonitric acid, 1 part of  $\text{HNO}_3$  and 3 parts of  $\text{H}_2\text{SO}_4$  are needed. To do so, a graduated cylinder needed to be used, in which it has been mixed 15 ml of nitric acid (1 part) and 45 ml of sulfuric acid (3 parts), to reach a total amount of sulfonitric acid of 60 ml. The acidic mixture was then poured into the becker containing the pristine nanotubes.

Now, the nanotubes immersed in the acidic mixture, were put into an ultrasonic bath ("SONICA-Ultrasonic Cleaner" by SOLTEC) and sonicated for the time needed for the functionalization desired to occur. The first solution of nanotubes and acid was unsightly for a time of 15 minutes, the second for a time of 30 minutes and so on, always increasing the sonication time for each solution by 15 minutes, up to 90 minutes of sonication in the ultrasonic bath.

Meanwhile, a solution of NaOH (sodium hydroxide given by "SIGMA-ALDRICH") and water has been prepared, which was used to neutralize the low pH of the acid solution and CNTs after the expected treatment in the ultrasonic bath. About 30 g of NaOH were inserted into a flask and then the flask was filled with water up to 200ml. This solution of sodium hydroxide and water was mixed using a magnetic stirrer ("ARE – Heating Magnetic Stirrer" of the "VELP® SCIENTIFICA") until the solution was completely homogeneous.

After the sonication process in the ultrasonic bath of the nanotubes immersed in acid, the contents of the becker were immediately poured inside the flask containing the basic solution of NaOH and finally the nanotubes were rinsed through the use of deionized water to avoid the formation of residual salts resulting from the neutralization reaction of the acid solution with the base. The final cleaning of the nanotubes was carried out many times in order to be sure that almost all the salt derived from the neutralization of the acidic solution was washed away in order

to avoid the risk of the salt present on the surface of the nanotubes acting as a negative element for the mechanical and electrical properties of the CNT-Cement composites



*Figure 27. Result of 30 minutes of sonication in the sulfonitric acid solution for CNTs*

## **6.3 CNT-CEMENT COMPOSITES**

### **6.3.1 CNT-CEMENT COMPOSITES PRODUCTION**

For the synthesis of the pure cement samples, a class 52,5 produced by Italcementi was used: this is a particular kind of Portland cement which shows a very high strength. The chemical composition for this type of cement is showed in Figure 1. This material was chosen because of its fast curing time, which allows it to reach the same hydration degree of a common Portland

cement hydrated for 28 days (standard time needed to reach at least 90% of hydration to guarantee the mechanical properties required).

For the synthesis process, it was assumed that the cement paste volume was equal to the sum of the cement powder volume ( $V_c$ ) and water volume ( $V_w$ ) used:

$$V = V_c + V_w = \frac{M_c}{\rho_c} + \frac{M_w}{\rho_w}$$

Where  $M$  and  $\rho$  are respectively the mass [Kg] and the density [Kg m<sup>-3</sup>]. Then:

$$V = M_c \left( \frac{1}{\rho_c} + \frac{x}{\rho_w} \right)$$

$$M_c = \frac{V}{\left( \frac{1}{\rho_c} + \frac{x}{\rho_w} \right)}$$

Where  $x$  is the water-cement ratio (w/c):

$$x = \frac{M_w}{M_c}$$

The value of the cement powder mass can be evaluate knowing the total volume of the system. In this case the total volume is the volume of the mold used to produce the cement specimen, which has a rectangular shape. It is formed by 4 identical molds that have width and thickness both of 2 cm and a length of 8 cm. So, the volume of a single mold is 32 cm<sup>3</sup> and the total volume of the mold, which is constituted of 4 identical molds, is 128 cm<sup>3</sup>.

For a more correct way to synthesize cement paste, it is advisable to use an excess of cement powder of 15%. This is explained by the fact that part of the cement paste inevitably remains attached to the surface of the walls of the mold. Hence, the final formula becomes:

$$M_c = 1,15 \cdot \frac{V}{\left(\frac{1}{\rho_c} + \frac{x}{\rho_w}\right)}$$

For the synthesis of cement paste for our samples, the water-cement ratio used was 0,45; that means that for a total volume of 147,2 cm<sup>3</sup> (value calculated considering the cement excess of 15%) the amount of cement mass to be used is  $M_c = 190,53$  g and the amount of water mass to be used is  $M_w = 85,74$  g.

Water and cement powder are then put in 2 separated becker and prepared for the mixing. In order to create the blend between the water and the cement powder, a mechanical stirrer (VELP® SCIENTIFICA “Stirrer type PW”) is needed. The becker containing the water is then put under the mechanical stirrer and the cement powder is added to the water by little amounts during the time, in order to create a homogeneous and smooth cement paste. After the mixing of the two elements is completed, the cement paste is poured into the mold, and after the excess of slurry is eliminated from the top of the mold so that the surface of the samples appears smooth.

Finally, the mold was put into an oven at the temperature of 85°C for 24 hours in order to accelerate the cement hydration process. Using this thermal treatment it can be achieved the same amount of hydration obtained by leaving the composite in water for 28 days, which is the traditional and conventional time for reaching almost 90% of hydration of the cement paste, time sufficient to show the best mechanical properties of the cement.

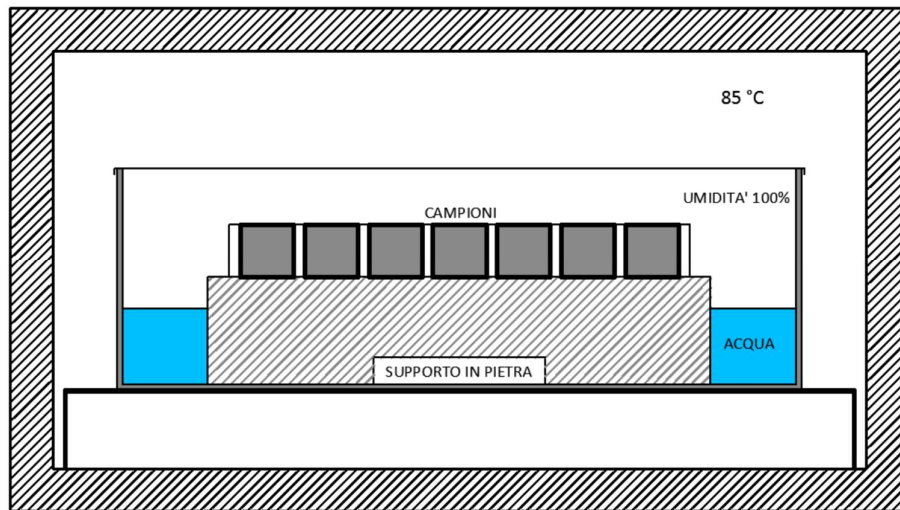


**Figure 21.** Scheme of the environment for the curing of the cement paste

## PRODUCTION OF CEMENT PASTE CONTAINING CNT

Regarding the production and preparation of concrete composites containing carbon nanotubes, the method is very similar compared to the production of the pure cement paste. However, the amount of carbon nanotubes chose as reinforcement in the cement composite samples was 0,1% referred to the cement powder mass used. In our study case, the mass of cement powder used for the pure cement paste was  $M_c = 190,53$  g so the mass of CNTs needed to be added to the water and cement is  $M_{CNT} = 0,19$  g.

Then, CNTs are added to the water and, in order to obtain the right dispersion of the solid phase (CNTs) in the water, an ultrasonic stirrer was used. This ultrasonic stirrer is composed by a probe located at the head of the instrument, which is immersed in the becker containing the water-CNTs solution. The time process of the ultrasonic dispersion of the nanotubes was 15 minutes, while the amplitude of the vibrations of the probe was set to be 35% with an energy released of 100 W.

After the dispersion of the carbon nanotubes was complete, the becker was filled up with water to reach the right amount of water needed to obtain a  $M_c M_w$  ratio of 0,45, which in this case was  $M_w = 85,74$ g.

### 6.3.2 GEOMETRICAL DENSITY

In order to measure the porosity within the samples, geometrical density values were calculated with the following procedure. It can be assumed that cement paste volume  $V$  is equal to the sum of cement powder volume ( $V_c$ ) and water volume ( $V_m$ ). As previously mentioned, the more water is present in the mixture, the more the cement particles are far from each other. So, when the paste is hardened and dried, this will result in a higher degree of porosity. Hence, for a given dry paste volume, there will be more “air gaps”, meaning a lighter sample with lower density.

The density [ $\text{Kg}\cdot\text{m}^{-3}$ ] calculated was the following:

$$\rho = \frac{M}{V}$$

Where  $M$  is the total mass of the dried sample and  $V$  is the total volume of the same, calculated by the product of the 3 sizes of the sample: width, length and thickness. Two measures on two different

### 6.3.3 RESISTIVITY

In order to evaluate the electrical behavior of the Carbon nanotubes inside the cement composites, an electrical test for the obtainment of samples resistivity has to be made. The instrument used for the electrical test generates a constant direct current flow that passes through the cylinder copper conductors couple, which in the middle of them was placed the sample. Moreover, the electric potential between the two conductors was measured by touching them with 2 testing probes linked to the instrument. By measuring those two parameters, the instrument gives directly the value of the resistance of the sample.

However, the surface of the sample subject to the current flow generated by the instrument is not equal to the surface of the 2 conductors made in copper. The reason is that the surface of the conductors is perfect circular with a diameter of 3 cm (the radii of the conductors are 1,5m), while the surface of the concrete samples in contact with the 2 cylindric conductors is a square which has a width of 2 cm.

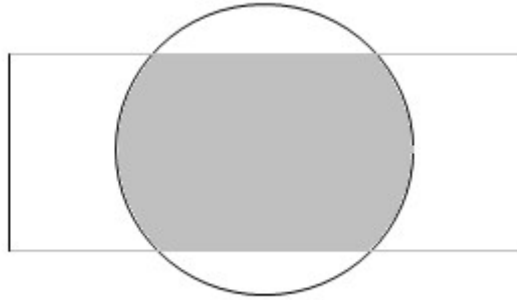


**Figure 28.** Area of the cement sample interested by the current flow for the resistivity calculation

The figure [] shows the area shared by the contact between the concrete sample and the copper conductor cylinder. The area in contact between the two materials shares only the central part (colored in grey) of the copper cylinder and this is the area in which the direct current flow through the material.

For the calculation of the interested area, we needed to subtract the 2 circular segments, located above and below of it, to the total area of the copper cylinder. The value of the diameter of the conductor cylinder is 3 cm, while the width of the concrete sample is 2 cm. Assuming that the 2 centers are located in the same point, the height of the circular segment is given by:

$$h = R - d = 1,5 - 1 = 0,5 \text{ cm}$$

where **R** is the circle radius and **d** is half of the width of the concrete specimen.

Then  $\theta$ , which is the angle formed by the circular segment, needs to be calculate in order to evaluate the area of it:

$$d = R \cdot \cos\left(\frac{\theta}{2}\right)$$

$$\theta = 2 \cos^{-1}\left(\frac{1}{R}\right) = 96,38^\circ$$

After obtaining the value of the angle, the area of the circular segment can be evaluated by the following equation:

$$A_{cs} = \frac{1}{2} R^2(\theta - \sin \theta) = 0,77 \text{ cm}^2$$

$$2A_{cs} = 2 \cdot 0,77 = 1,54 \text{ cm}^2$$

Where  $A_{cs}$  is the area of one circular segment.

Then, for the calculation of the interested area, the area of the two circular segments need to be subtracted from the total area of the copper circle:

$$A_{cc} = \pi R^2 = 7,07 \text{ cm}^2$$

$$A = A_{cc} - 2A_{cs} = 5,53 \text{ cm}^2$$

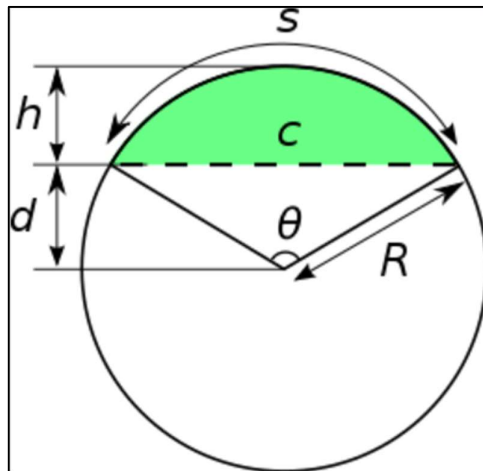


**Figure 29.** Circular segment

## 6.4 MECHANICAL TESTS ON CNT-CEMENT COMPOSITES

### 6.4.1 THREE-POINT FLEXURAL TEST

The main task for this experimental work was to test the CNTs-cement composite samples that were previously prepared by mixing carbon nanotubes, which were functionalized at several sonication times in a sulfonitric acid solution, by a flexural testing machine with a load cell having a maximum capacity of 1kN. In this case the machine used to test the samples consisted in a single-column Zwick/Roell-line Z050 flexural testing machine, as showed in Figure []. The mechanical properties of the cement composites were measured through a three-point bending test (the standard controlling the variables of the test was the ASTM C348) controlled by Crack Mouth Opening Displacement (CMOD). CMOD is a term used to describe the change in distance, normal to the crack plane, between the two faces of fatigue-cracked notch in a fracture toughness test specimen. CMOD is measured on the loading line or on the surface of the specimen as the difference between the original and the final crack opening.

For the specimens tested in order to evaluate the Max stress at breaking and the toughness, a span of 65mm between the two supports at the bottom of the machine was set. The test was set to begin when a force of 10 N was applied on the top surface of the specimen by the top bar of the machine. On the other hand, the test was stopped when the force applied by the top bar reached a value of 10% of the maximum value of force measured by the machine.

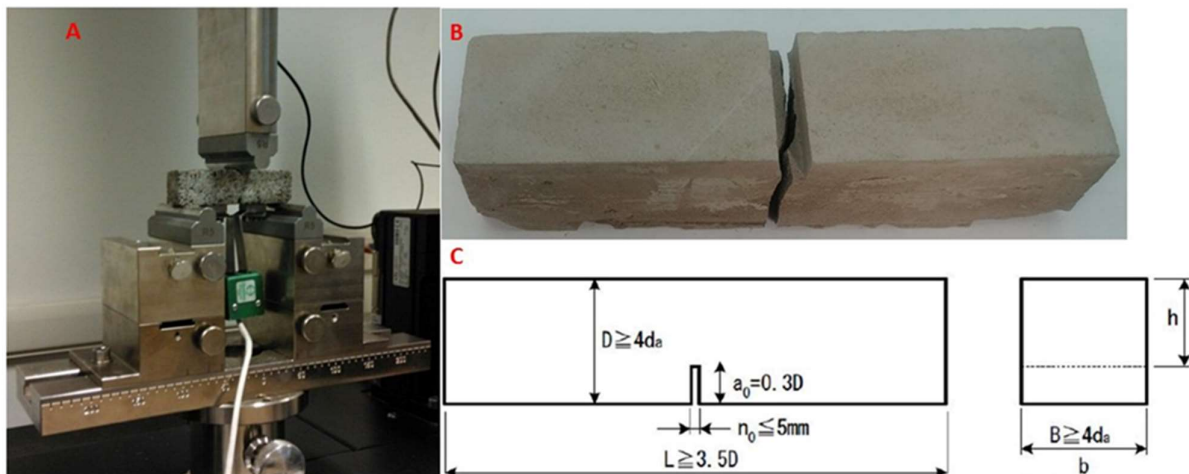


**Figure 30.** Geometry of the specimen used in the flexural strength test with the respective size and notch dimensions

The software used to evaluate the data coming from the bending test was testXpert II. The data reported by the software from the completed tests are: maximum force ( $F_{max}$ ), elongation measured when the maximum force is applied (dL at  $F_{max}$ ), force measured at break of the specimen ( $F_{break}$ ), elongation in mm measured at break of the specimen (dL at  $F_{break}$ ).

The software also permits to indicate the thickness and the width of the specimen in order to calculate the fracture surface.

Also, the test was conducted in a way that every 0,05 mm the value of Force (in N) applied on the specimen is recorded. This method allows the calculation of the maximum Stress (in MPa) distribution in the interval of 0,05 mm by this equation:

$$\sigma_{0,05} = \frac{3F_l L}{2bh^2} \left[ \frac{N}{mm^2} \right]$$

Where:

- $F_l$  is the maximum force registered in the interval of 0,05 mm of displacement.
- $L$  is the span of the specimen (65 mm).
- $b$  is the width of the specimen in mm.
- $h$  is the thickness of the specimen subtracted by the size of the notch on the surface.

The displacement is measured through an extensometer which is installed above the notch of the sample and it is attached to two supports glued to the notch surface spaced 20 mm from each other. This type of configuration is showed in Figure 33.

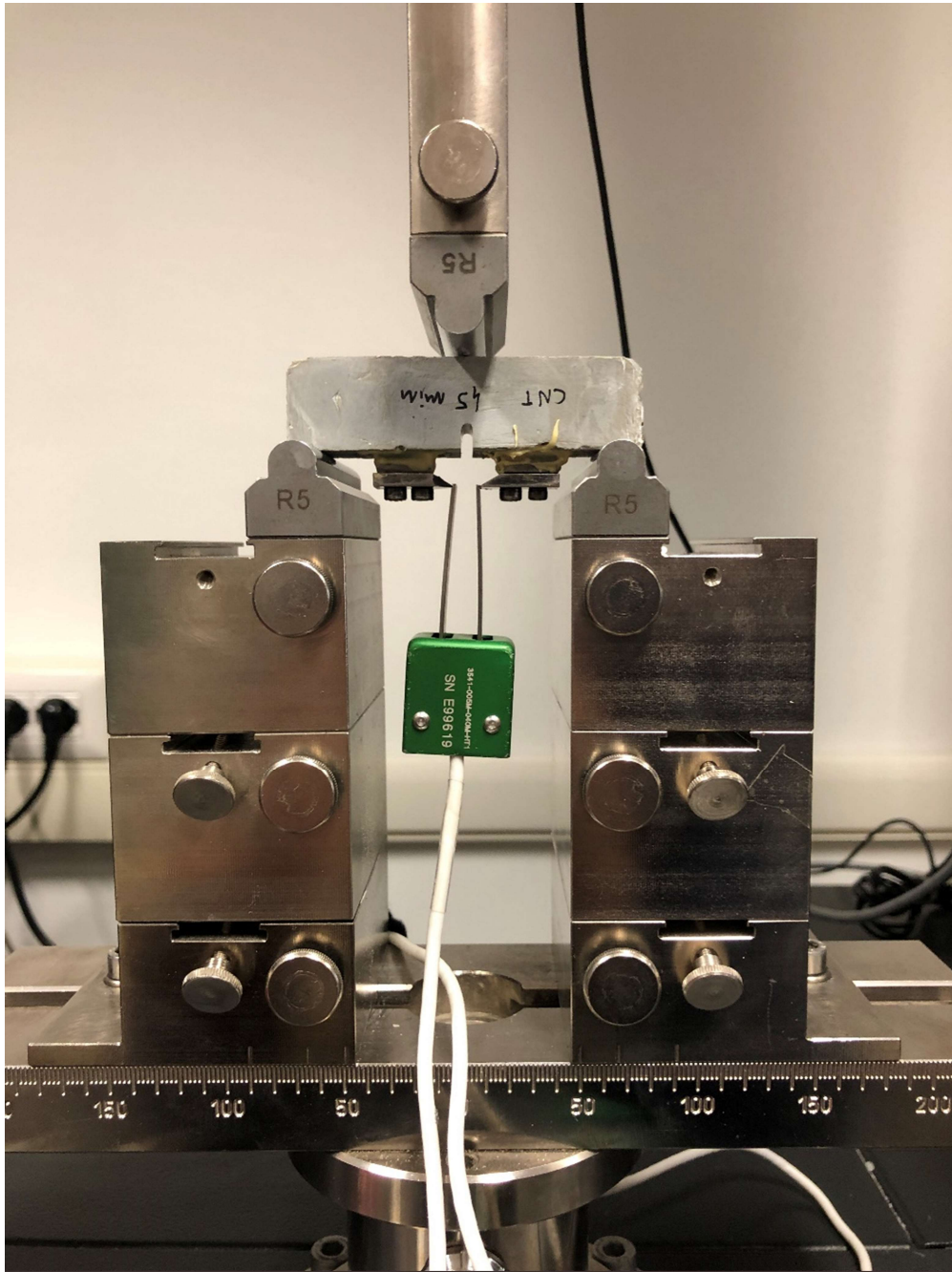


*Figure 31. Extensometer configuration for the three-point test*

#### 6.4.2 COMPRESSIVE TEST

The second kind of mechanical test carried out for the CNT-cement composite samples was the compressive strength evaluation. The compressive test was conducted through two different ways: the first one using “force control” and the second one using “elongation control”. The load cell had a maximum capacity of 50 kN, The samples were placed in the middle of two presses, the upper one is the mobile one, moved by the bar placed on top of it, while the second press is stationary and it is placed under the composite sample. The test, in fact, evaluates the Max stress at which the CNT-cement composites samples are broken by the compression applied by the two presses. In the elongation control method, the compression test was carried out by increasing the displacement of the 2 presses in a constant way; on the other hand, the force control method consisted in increasing the force applied by the machine in an instantaneous way until the sample was broken and then measuring the maximum force reached at that point.

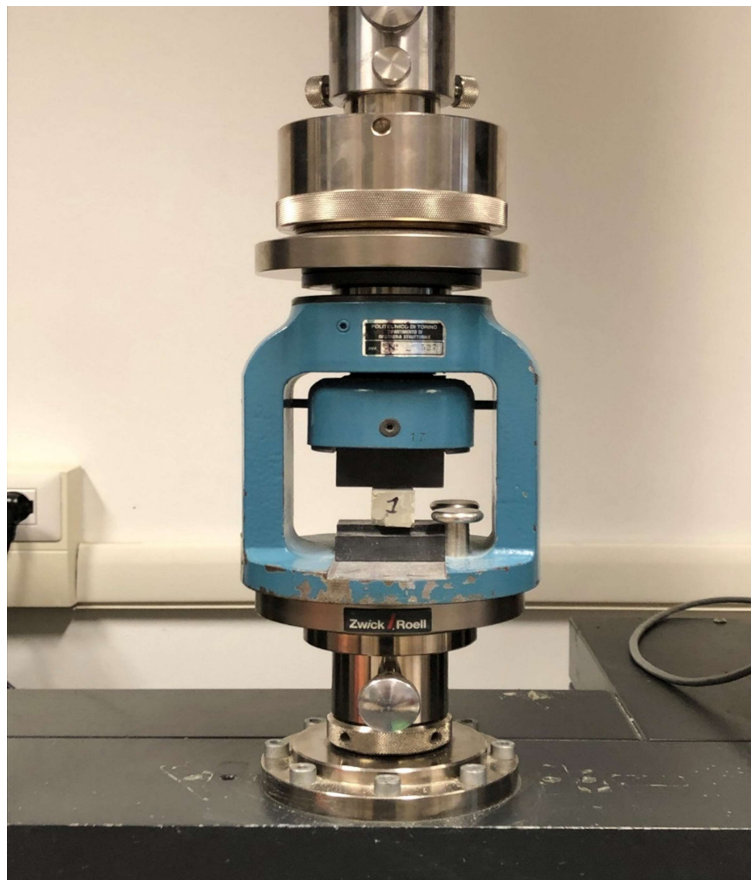


*Figure 32. Picture of the compression test environment.*

## 7. RESULTS AND DISCUSSION

### CARBON NANOTUBES CHARACTERIZATION

#### THERMOGRAVIMETRIC ANALYSIS

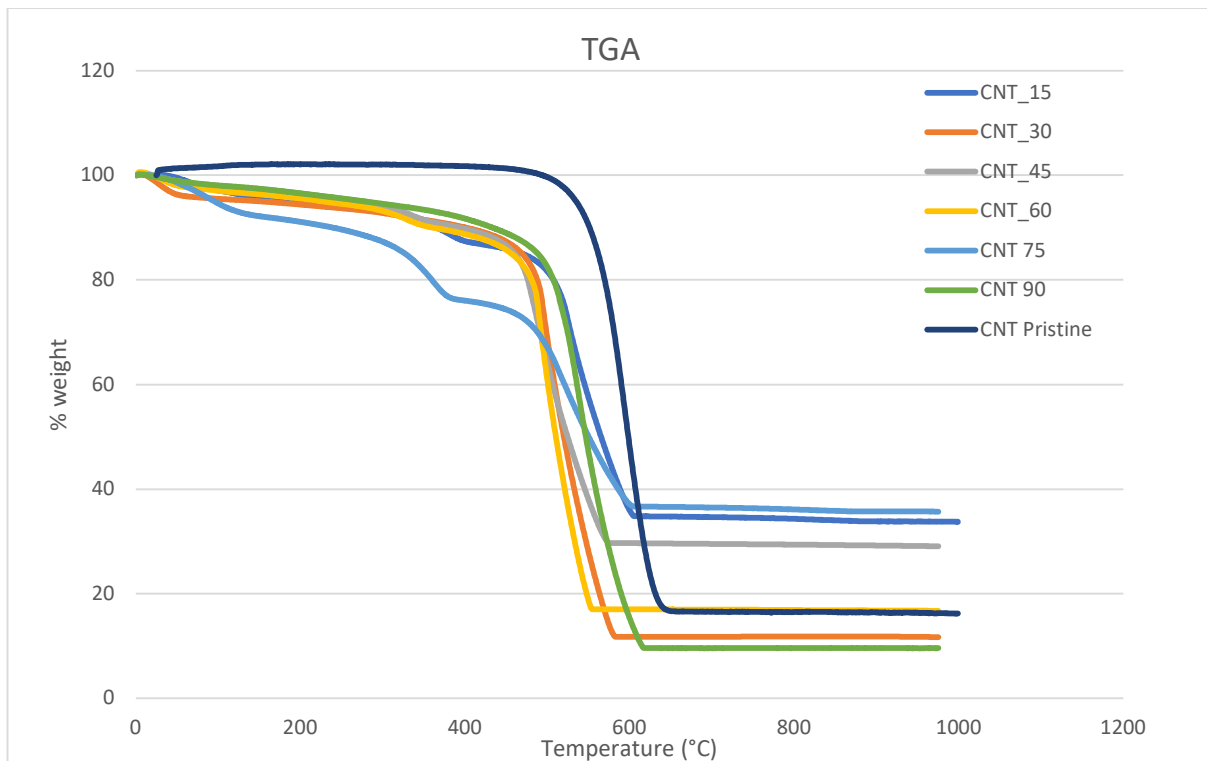


**Figure 33.** Graph showing TGA curves of carbon nanotubes functionalized at several sonication times

In order to characterize the thermal behavior of the carbon nanotubes, after chemical functionalization in the sulfinitric acid solution ( $1 \text{ HNO}_3 : 3 \text{ H}_2\text{SO}_4$ ) at different sonication times, used for the preparation of the CNT-Cement sample, a ThermoGravimetric Analysis (TGA) was conducted. From figure 36, which shows the curves obtained from TG analysis in an air atmosphere with a gas flow of 50 ml/min and a temperature ramp of 10 °C/min, it can be seen that: in general, non-functionalized carbon nanotubes have an onset temperature of thermal degradation around 525 °C and a maximum degradation rate at a temperature of 600°C. The

complete degradation of non-functionalized nanotubes occurs at a temperature of about 630°C. On the other hand, when talking about the analysis of the functionalized CNTs, unlike the pristine nanotubes, the onset temperature of the degradation for the least sonicated nanotubes (in this case the nanotubes sonicated for 15') is 480 °C, which is way below the temperature at which the pristine nanotubes begin to degrade. This is followed by the fact that almost all the curves related to the functionalized CNTs are really close to each other regarding their degradation temperature. Anyway, it can be seen that increasing the sonication time, the onset temperature of degradation decreases as a consequence of the presence of oxygenated functional groups attached to the carbon nanotubes surface. Also, this can be explained by the fact that oxygenated groups are chemical species that are very reactive and temperature sensitive, so the more those species are present on the carbon nanotube surface, the more the nanotubes start their degradation at lower temperatures.

It can also be seen that the percentage of residue present at the end of the degradation for the functionalized CNTs is generally higher than the one showed by the pristine nanotubes. In fact, the samples functionalized for 15 and 75 minutes show a residue of about 35%, while the pristine carbon nanotubes have a residue of less than 20% at the end of the analysis. The explanation lies in the fact that, regarding the functionalized samples, there is still a good amount of salts derived by the reaction between the sulfonitric solution and the basic one [86]. These salts have a better thermal stability than the CNTs even at the maximum temperature of the Thermogravimetric analysis (1000°C), so, they are still present even if the thermal degradation of the CNTs has already ended.

In addition, the curves representing functionalized carbon nanotube samples have an initial decrease, so an early step of additional degradation compared to pristine CNTs. This step can be attributed to the presence of water molecules present on the surface of nanotubes. In fact, these molecules are used to being eliminated in a fairly low temperature range of about 100 to 300°C. This phenomenon is very clear when analyzing the sample sonicated for 75 minutes, which shows more than 20% loss in weight due to the elimination of water.

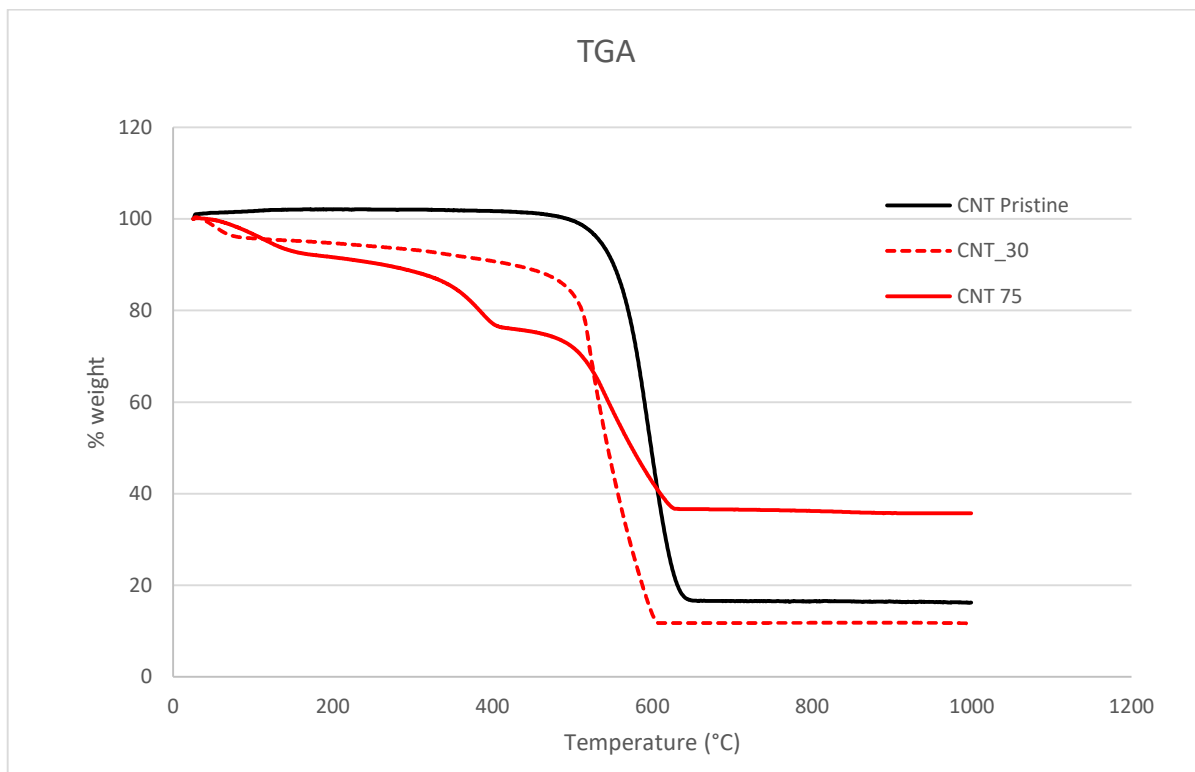


**Figure 34.** Difference in decomposition starting temperature for: Pristine carbon nanotubes, carbon nanotubes sonicated for 30 minutes, carbon nanotubes sonicated for 75 minutes

### RAMAN SPECTROSCOPY

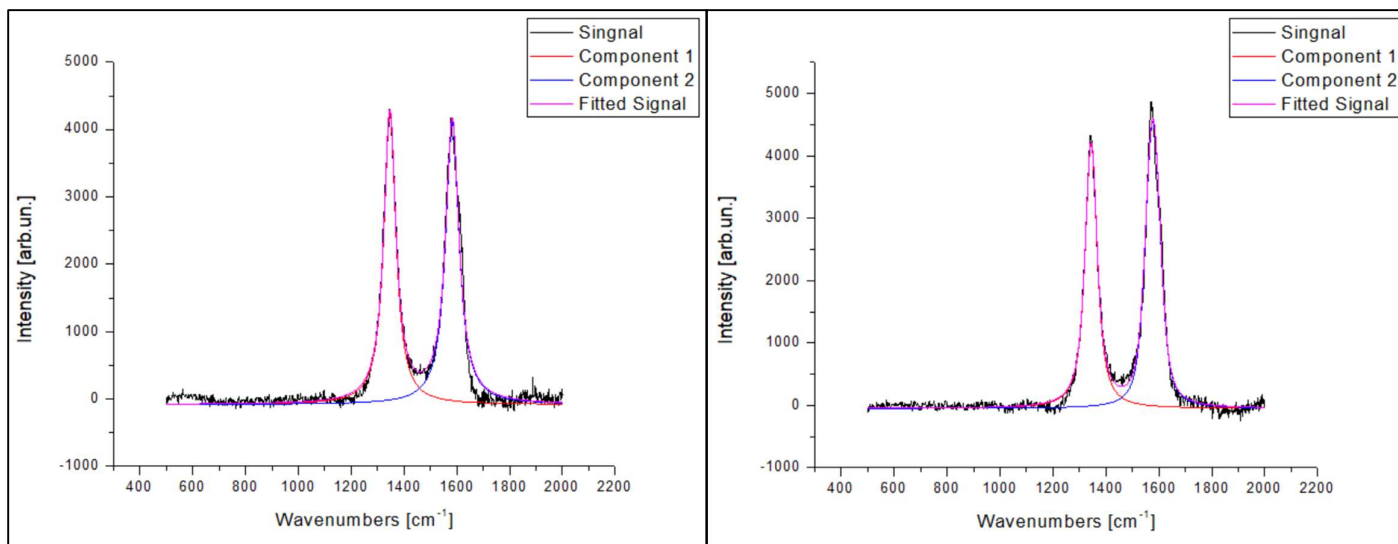


**Figure 35.** Comparison between Raman spectrum for nanotubes functionalized for 60 minutes (left) and nanotubes functionalized for 15 minutes (right)

The typical Raman spectrum for the functionalized CNTs (Figure 12) generally shows two different bands, one located at 1300-1350  $\text{cm}^{-1}$ , which is called “Defect band” (D) and one located at 1600  $\text{cm}^{-1}$ , which is called “Graphitic band” (G) [89]. It can also be seen that, comparing two different spectrum regarding two different sonication times of carbon nanotubes (15 and 60 minutes), the D band (colored in red) intensity is slightly bigger for the one functionalized for 60 minutes compared to the one functionalized for 15 minutes.

However, in order to evaluate the effectiveness of the covalent functionalization of the carbon nanotubes in the  $\text{HNO}_3$  and  $\text{H}_2\text{SO}_4$  acidic solution, it must be considered the relative intensity ratio between D and G bands. This ratio is called IG/ID ratio and gives a fairly good quantitative information about the amount of -COOH groups present on the surface of CNTs. In fact, the more intense is the D band compared to the G band, the more oxygenated groups are attached to the nanotubes surface.

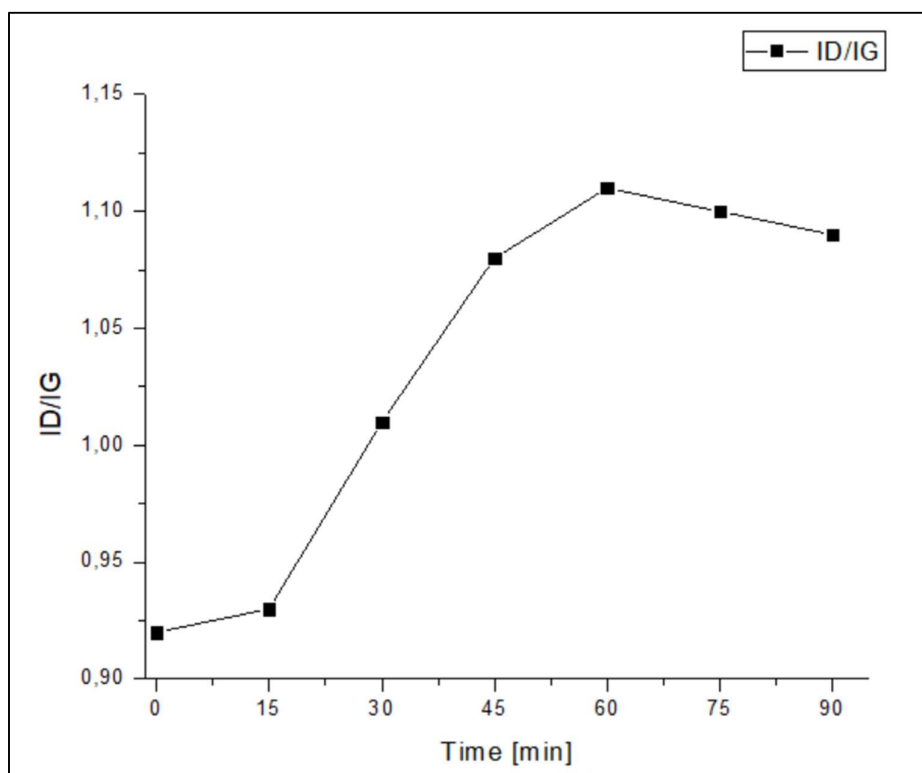


**Figure 36.** Graph showing the ID/IG ratio for every functionalized CNT sample

As mentioned before, Raman spectroscopy results are evaluated with the ID/IG ratio. This ratio is taken as a measure of the influence of the degree of functionalization of the CNTs. In fact, as showed in Figure 35, the more time CNTs are immersed in the acidic solution, the bigger is the ID/IG ratio. This can be explained by the fact that increasing the functionalization time also increases the number of -COOH groups present on the nanotubes surface. However, this trend is valid only for times lower or equal to 60 minutes, where the maximum value of the  $I_D/I_G$  ratio is located. After that, no further increase or even a decrease in the  $I_D/I_G$  ratio is observed for higher defect concentration regarding the 75 and 90 minutes functionalization. This decreasing in  $I_D/I_G$  ratio can be related to the fact that for a longer period of functionalization the structure of the nanotubes seems to be a bit damaged by the reaction with the acidic solution.

### FLEXURAL STRENGTH

Sample N°	Name	Max stress (MPa)	Standard Deviation
1	OPC 1	1,5	±0,2
2	CNT pristine	1,6	±0,1
3	CNT 15 min	1,8	±0,1
4	CNT 30 min	2	±0,2
5	CNT 45 min	2,1	±0,5
6	CNT 60 min	3,9	±0,4
7	CNT 75 min	4,5	±0,8
8	CNT 90 min	4,7	±1,1

*Figure 37. Values of max stress at breaking for CNT-cement samples with the relative error*

From the values of max stress at breaking evaluated by the flexural strength test reported in the table of the Figure 38, first it can be seen that the difference in max stress measured between the ordinary Portland cement sample (1,52 MPa) and the sample containing pristine carbon nanotubes (pure CNTs non-functionalized) (1,57 MPa) is very small. This result can be explained by the fact that the dispersion of pristine carbon nanotubes inside a cement matrix does not lead to an improvement in mechanical properties since the interaction between the reinforcement and the matrix seems to be weak.

However, increasing the time of acidic functionalization through sonication, the max stress at breaking point evaluated by the flexural tests also increases and becomes twice or three times the value of the one measured for the pristine CNTs in the concrete. As it can be seen from the table in figure 37, the increasing of the functionalization time leads to an increase in the max stress at breaking point in almost a linear way, which tends to end in a plateau for functionalization times of 75 minutes and 90 minutes.

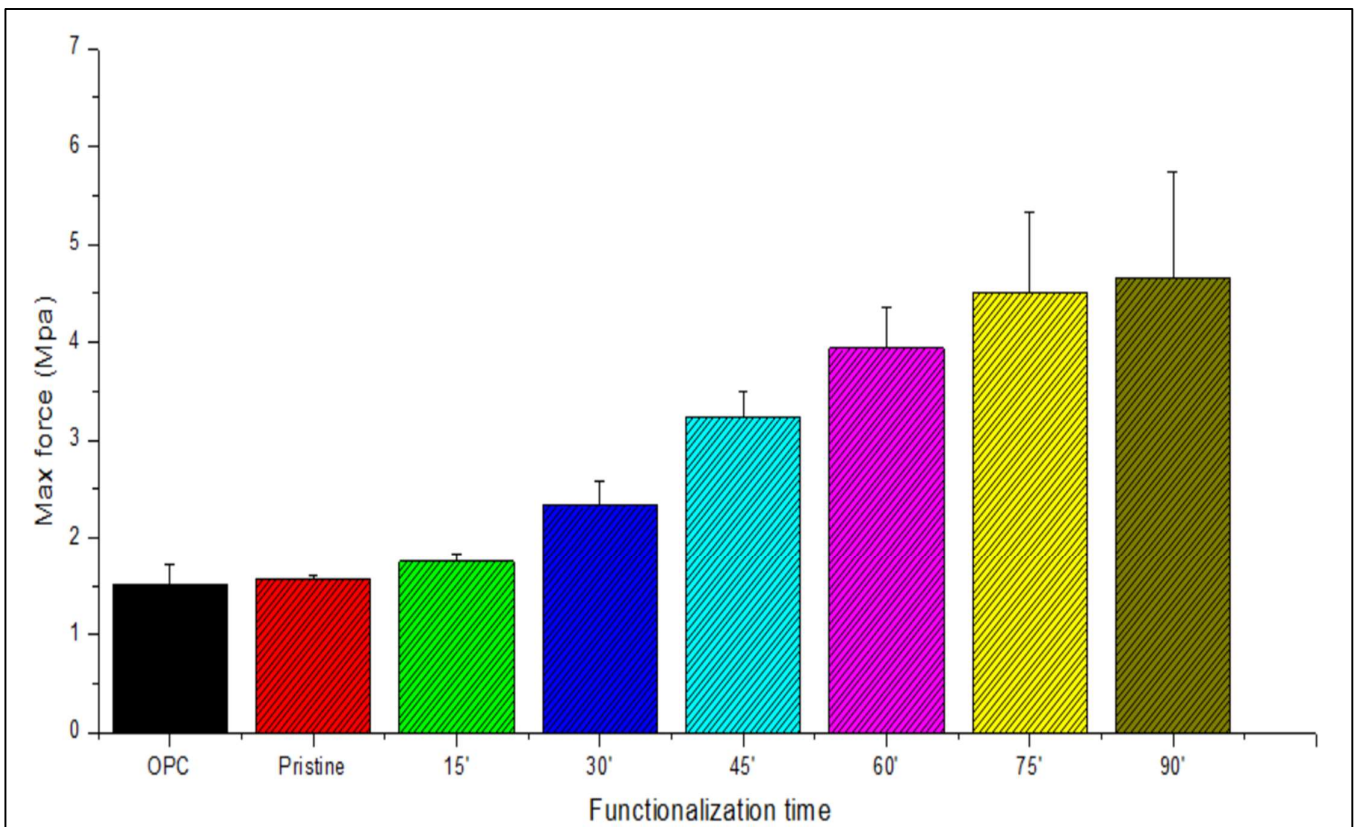


**Figure 38.** Bar chart reporting the values of Max stress for every samples of CNT-cement composite

From the graph in Figure 39, it can be seen that the flexural strength for the CNT-cement composite in which were dispersed the nanotubes sonicated for 15 minutes only increases by 15% compared to the strength of the Ordinary Portland Cement (OPC). However, the sample containing the 45' CNTs shows an increase in flexural strength, always in relation with the OPC sample, of about 40%, while regarding the 60' CNT sample the value increases even of 160%.

This flexural strength enhancement can also be related to the  $I_D/I_G$  ratio already discussed in the Raman spectroscopy characterization. In fact, for lower degrees of functionalization the trend of the Max force evaluated in the composites is very similar to the one showed by the Raman spectroscopy, or else, the enhancement brought by the presence of the right amount of oxygenated groups on the CNTs surface is showed by the 60 minute functionalization time. Analyzing, instead, the 75 and 90 minutes functionalization, the flexural strength enhancement is still visible but with less effectiveness than the one evaluated for the nanotubes sonicated for 60 minutes. Probably, the fact that the 75' and 90' samples tend to a maximum plateau value of flexural strength is caused by a very slight agglomeration of the nanotubes inside the cement matrix due to the interaction between the functional groups and  $Ca^{2+}$  ions present in the cement paste and causing the formation of higher amount of ettringite.

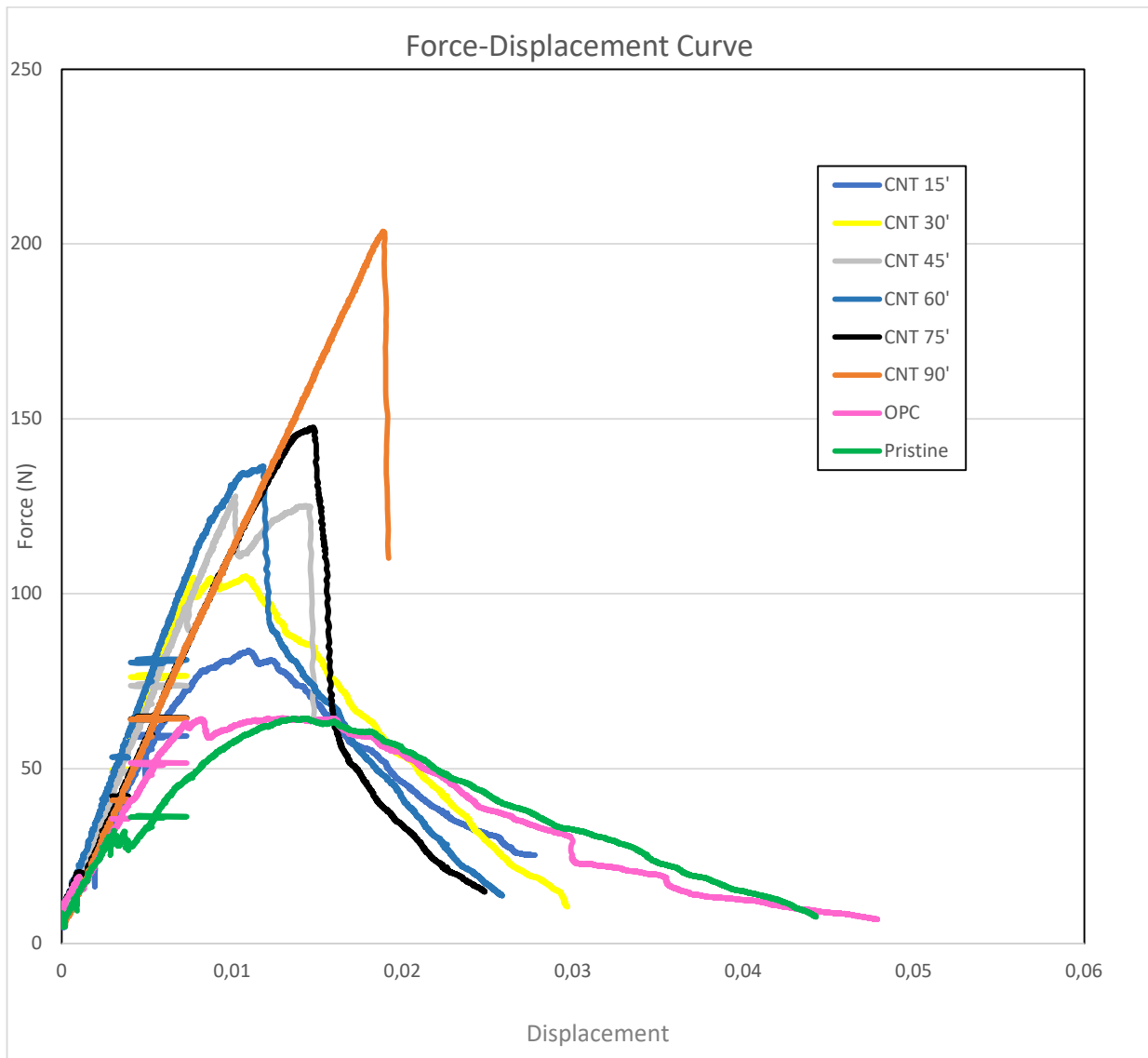


**Figure 39.** Graph showing every flexural test curve for all the CNT-concrete composite samples tested

In the Figure 17 it is shown the graph Force-Displacement of the various samples tested in the DISEG laboratories of Politecnico di Torino. These curves demonstrate the already discussed behavior of the CNT-cement composites adding 0,1% of functionalized CNTs for different periods of time. By increasing the sonication time, the maximum force endured by the samples also increases; however the integral of the curves also become slightly lower when increasing the functionalization time leading into a decrease in fractural energy, showing that with the same amount of CNTs used as a reinforcement for the cement matrix (0,1%) but increasing the fraction of functional groups to the CNT surface, causing an evident improvement regarding the maximum loading, but showing a small reduction in the composite fracture energy.

This mechanical improvement because of the combination of CNT filler, nucleation, bridging effect and the consequent densification of the cement paste, leading to a reduction of total porosity and pore continuity. This bridging effect is very much improved when the number of chemical groups attached to the CNT surface increases by increasing the functionalization time, ensuring a better interaction between those oxygenated groups and the C-S-H contained in the cement.

## COMPRESSIVE STRENGTH

Sample N°	Sample name	Max stress (Mpa)	Standard deviation
1	OPC	48,6	±7,9
2	Pristine	50,8	±2,5
3	15'	48,2	±10,9
4	30'	49,9	±3,3
5	45'	52,2	±4,1
6	60'	52,5	±8,2
7	75'	54	±5,3
8	90'	56,4	±10,5

**Figure 40.** Table showing the compression strength for all the composite samples.

The third test carried out in order to evaluate the total mechanical behavior for the CNT-cement composites is the compressive strength. From the table showed in Figure 39, it can be observed that the values of maximum stress don't change that much for the functionalized CNTs samples compared to the OPC values. Specifically, the maximum compressive strength evaluated for the ordinary Portland cement is 48,6 MPa, while the value for the pristine CNTs is 50,8 Mpa, showing an increase of about 5% in compression strength. However, the addition of CNTs functionalized for 15 and 30 minutes doesn't bring to a considerable change in compressive strength (48,2 and 49,9 MPa respectively). Anyway, the samples showing the best compression strength are once again

the one with the CNT sonicated for 60, 75 and 90 minutes with a maximum compression strength respectively of 52,5, 54 and 56,4 Mpa.

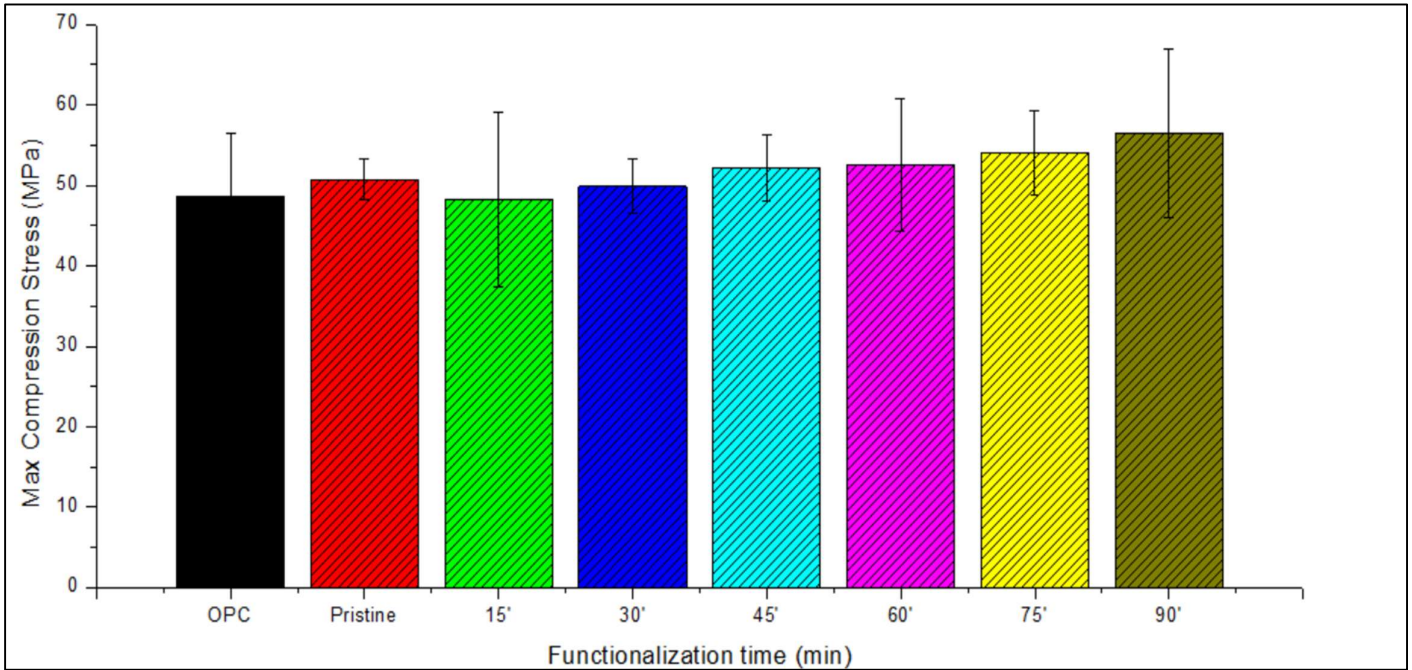


**Figure 41.** Comparison of compressive strength of all the CNT-cement samples tested by a compression machine

As shown in Figure 41, the values of maximum compression strength of all the samples doesn't vary much from the one obtained for the OPC sample. In particular, the best increment in compression strength is shown by the composite containing the nanotubes sonicated for the most time (90 min) with an increase compared to the OPC sample of only about 16%. This result, in relation with the results obtained in the flexural strength test, can be explained by the fact that the strengthening effect due to the dispersion of functionalized CNTs inside the cement matrix may be mostly present in the central part of the sample (explaining the fact that the flexural strength was enhanced when increasing the sonication time of carbon nanotubes in the 1 HNO<sub>3</sub> : 3 H<sub>2</sub>SO<sub>4</sub> solution), while the dispersion was not so optimal in the areas close to the lateral walls of the composite sample. This difference in dispersion of the 0,1% in volume fraction of the carbon nanotubes can bring to the conclusion that when evaluating the strength on the entire composite sample, the values don't increase in a considerable way in comparison with the evaluation of the flexural strength which takes place in the area around the notch of the sample, where the dispersion of the reinforcement seems to be optimized.

Anyway, from the observation of the values, even if the improvement brought by the 75' and 90' functionalized CNTs to the composite is very low, it can be said that, as already said for the results obtained by the flexural strength evaluation, the better interaction between the CNTs with the most amount of -COOH groups at the surface and the cement matrix helps improving the compression strength overcoming the negative effect on the mechanical strength due to the poor distribution and dispersion of the reinforcing phase (CNTs).

## FRACTURE ENERGY

Sample N°	Sample name	Fracture energy (J)	Standard deviation
1	OPC	1,3	±0,5
2	Pristine	1,4	±0,3
3	15'	1,6	±0,1
4	30'	1,5	±0,2
5	45'	1,6	±0,5
6	60'	1,7	±0,1
7	75'	2	±0,4
8	90'	2,4	±0,7

**Figure 42.** Table with the values of Toughness evaluated by the flexural test.

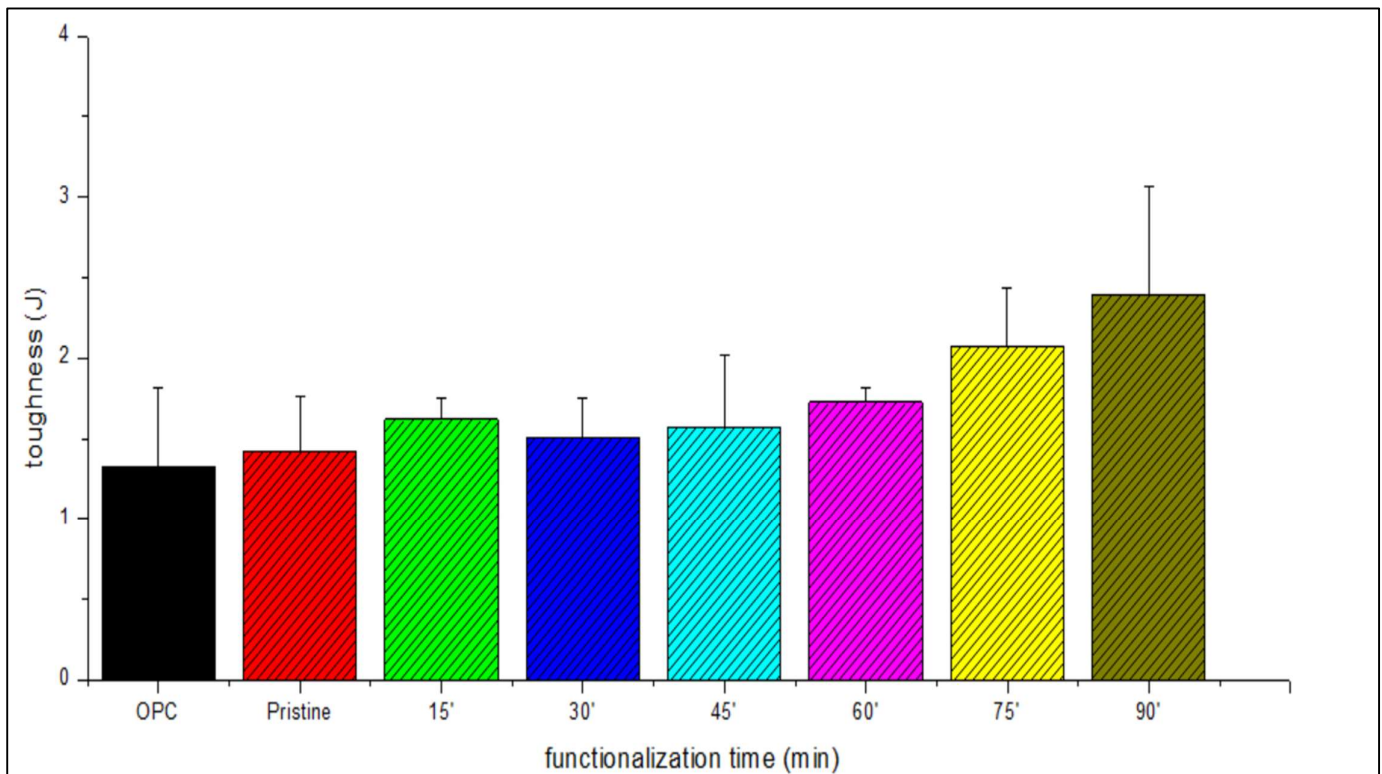


**Figure 43.** Bar chart showing the difference in Fracture Energy for the CNT-composite samples

The Fracture energy was evaluated by calculating the area under the curve of the respective CNT-cement composite samples. As shown by the bar chart in Figure 43 and the flexural strength values reported in Figure 42, it is possible to affirm that the CNTs functionalization time contribute to enhance the fracture energy of the composites. These results suggest an effective dispersion and a strong bond between carbon nanotubes and the cement hydration products by increasing the acidic functionalization time. In fact, the CNTs functionalized for 90 minutes bring an enhancement in fracture energy of 71% compared to the one measured for the pristine CNTs. Also, even the CNTs functionalized for 75 minutes shows an increase in fracture energy, always compared to the one evaluated for the pristine CNTs, of 43%.

## RESISTIVITY

Sample N°	Sample name	Resistivity ( $10^6$ m/S)
1	OPC	3,7
2	Pristine	3,6
3	15'	3
4	30'	3,3
5	45'	1,9
6	60'	1,1
7	75'	0,5
8	90'	0,1

**Figure 44.** Table with the resistivity comparison between functionalized CNT-cement composites

As showed in the Figure, an increasing in electrical properties brought by the insertion of functionalized carbon nanotubes inside the cement matrix can be observed. In particular, the value of resistivity for the OPC (ordinary Portland cement) sample is pretty similar to the one evaluated for the sample containing pristine (non-functionalized) nanotubes. This result can lead to the fact that only with the addition of 0,1% of CNTs not sonicated but dispersed into the cement matrix doesn't prove to be an improvement regarding the electrical properties. Meanwhile, increasing the functionalization times, the value of resistivity evaluated for the several CNTs-cement composites was decreasing. In particular, the decrease in resistivity between the 30' sonicated CNTs and the 45' sonicated CNTs was about 73%, showing a heavy enhancement in electrical properties of CNTs-cement composites even by increasing the functionalization time of 15 minutes. Also, the best result I brought by the composite containing carbon nanotubes functionalized for 90 minutes, which show an increase in conductivity of 3500% compared to the composite containing just the pristine CNTs.

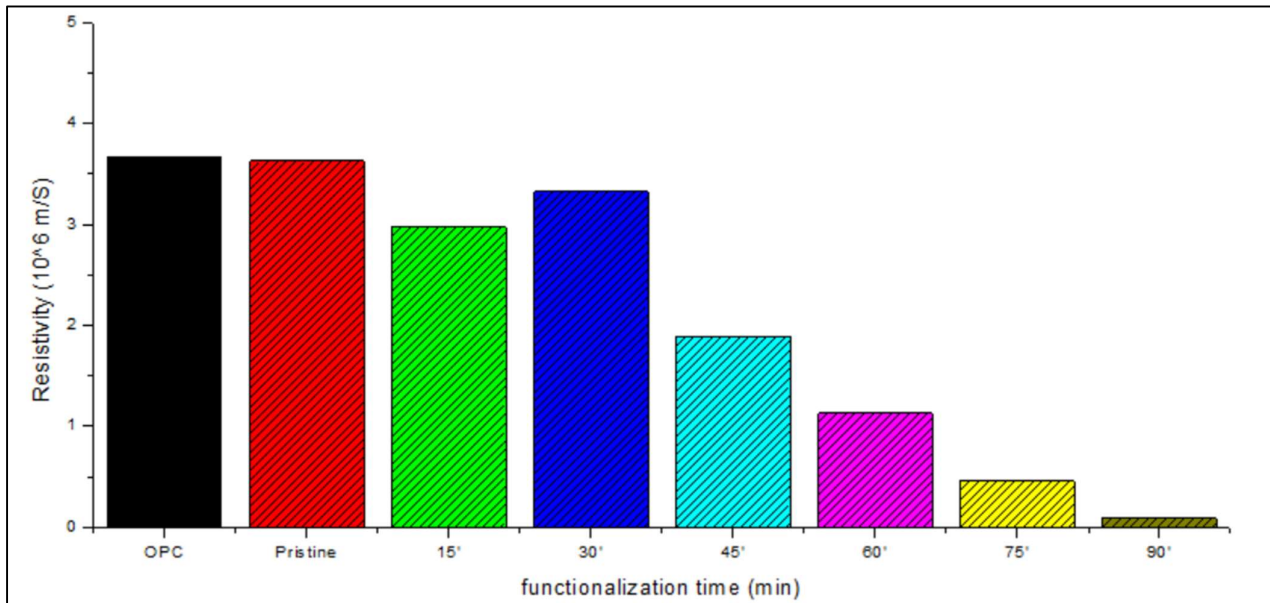


**Figure 45.** Effect of functionalization time of CNTs on the resistivity of the composite

From the graph above (Figure 42), showing the electrical properties of the concrete composites with 0,1% of carbon nanotubes inside the cement matrix, in particular the resistivity of the specimens tested, it can be seen that the resistivity of the samples decreases while increasing the time of functionalization of the carbon nanotubes inside the composite.

In particular, it can see that for the OPC and the CNT pristine (not functionalized) composite the resistivity is capped at a certain value, which is about  $3,7 \cdot 10^6 \Omega \cdot \text{m}$  for the ordinary Portland cement sample and  $3,6 \cdot 10^6 \Omega \cdot \text{m}$ ; that is because the value of electrical resistance measured by the instrument reached the maximum measurable value for this two samples. Instead, the 15' sonicated CNTs seem to have a lower resistivity (that means better conductivity) than the 30' sonicated CNTs. However, from the 45' sonicated carbon nanotubes it can be seen a drastic decrease in resistivity, following a trend dictated by an increasing of the functionalization time of the nanotubes inside the composites. In fact, samples containing nanotubes functionalized at times greater than 75 minutes show very low resistivity values, which go down to  $0.09 \cdot 10^6 \text{ m/S}$ .

However, the combination of the enhancement in mechanical properties with the increasing in electrical conductivity of the functionalized CNT-cement composites depending on the time of functionalization leads to considering these CNT-cement composites as an optimal and very efficient sensing devices that can be used in controlling the building deformations.

## GRAPHENE-LIKE COMPOSITES MECHANICAL TESTS

### FLEXURAL STRENGTH

The last part of the experimental work performed in the Department of Science and Technology of the Politecnico di Torino consisted in evaluating the mechanical properties of graphene-like and cement composite samples in relation with the mechanical properties of the samples already tested.

The method used for estimating effect of graphene inside the cement matrix was almost equal to the one used for the CNT-cement composites. The main difference is that no functionalization was performed for the graphene, because we wanted to see the mechanical properties for a pristine graphene. Also, the amount of graphene that was added to the cement paste was 0,1%, which is the same amount used for the CNT-cement composites in the previous work.

The results coming from the CMOD flexural strength tests, showed that the max stress at breaking measured for the graphene-cement composites is of about way better than those showed by the CNT pristine immersed in the cement matrix. In fact, the graph below indicates that the strength of the graphene is comparable with the strength showed by the carbon nanotubes sonicated in sulfunitric acid solution for 45 minutes.

Sample	Name	Max Stress [MPa]	Standard deviation
1	OPC	1,52	± 0,19
2	Soot Pristine	2,79	± 0,49
3	CNT Pristine	1,57	± 0,04
4	CNT 90'	3,23	± 0,26

**Figure 46.** Comparison of Flexural strength between the graphene-cement composite and CNT-cement composites

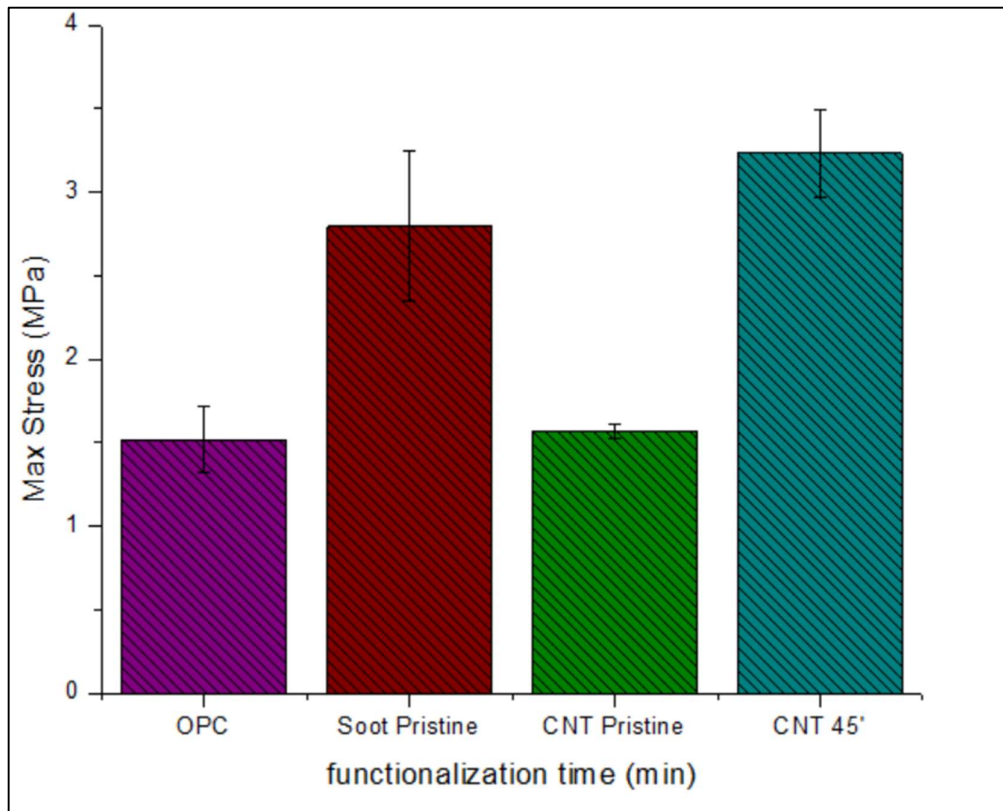


**Figure 47.** Bar chart showing the flexural strength of the tested samples

## FRACTURE ENERGY

Regarding the toughness measured for the same graphene-like-cement composites sample, the results seem even better. In fact, this time, the values of toughness for a pristine graphene inside the cement matrix overcome even the values of CNTs sonicated in the sulfonitric acid solution for 90 minutes by increasing the toughness value even of 18%. Moreover, using graphene-like nanoparticles inside the cement matrix, improve by 100% the fracture energy compared to the pristine CNTs inside the cement composited.

This result can be translated in the fact that the nanocomposite formed by cement as the matrix and graphene as the reinforcement phase, in general, shows much better mechanical properties than the nanocomposite formed by functionalized CNTs as the reinforced phase.

Sample N°	Sample name	Toughness (J)	Standard deviation
1	OPC	1,3	± 0,49
2	Soot Pristine	2,8	± 0,99
3	CNT Pristine	1,4	± 0,33
4	CNT 90'	2,4	± 0,67

**Figure 48.** Table showing the toughness measured for the graphene-cement composite and the CNT-cement composite.

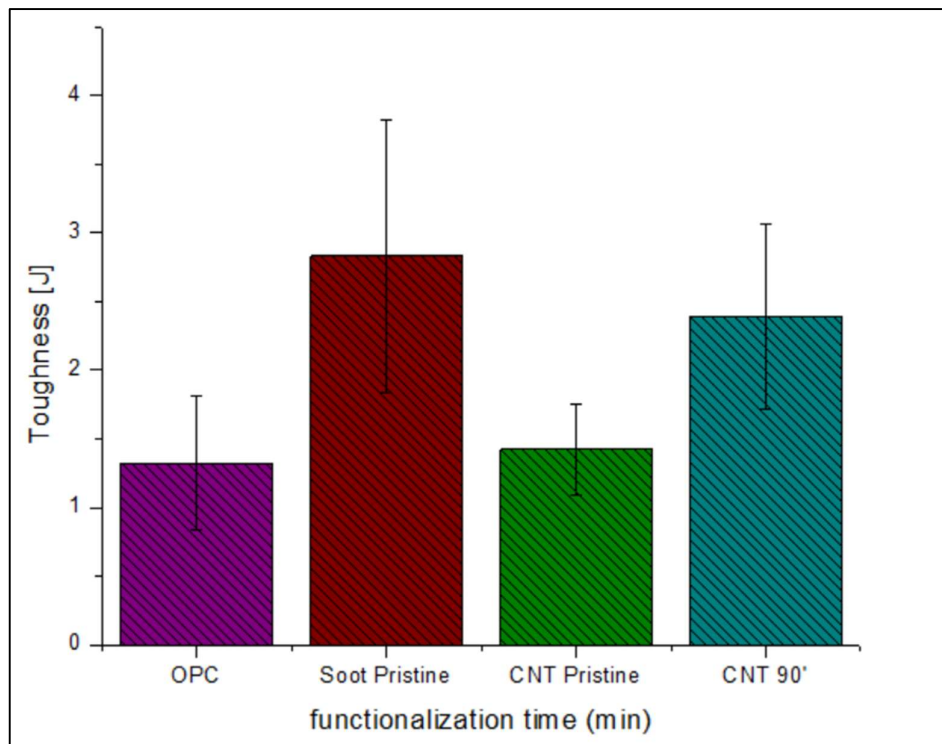


**Figure 49.** Bar chart showing the difference in toughness for the tested samples.

## COMPRESSION STRENGTH

The last results that need to be discussed regarding the mechanical properties of the CNT-cement composites is the compressive strength. As showed by the table in Figure 50 and by the bar chart in Figure 51, the maximum compression stress evaluated for the pristine CNTs-cement composite was 55,8 MPa, while the one measured for the graphene-like-cement composite was 50,8 MPa, showing an increase in compression strength of almost 10%. Moreover, it can also be seen that the value of compressive strength showed by the graphene-like composite is comparable with the one measured for the CNTs-cement composite containing CNTs functionalized for 90 minutes. In fact, the difference between the maximum compression stress for CNTs functionalized 90' and the maximum compression stress for the graphene was only about 1%.

Sample N°	Sample name	Max Stress (Mpa)	Standard deviation
1	OPC	48,6	±7,9
2	Soot Pristine	55,8	±2,9
3	CNT Pristine	50,8	±2,5
4	CNT 90'	56,4	±10,5

**Figure 5012.** Comparison between the maximum compression stresses for graphene like-cement composites and CNT-cement composites.

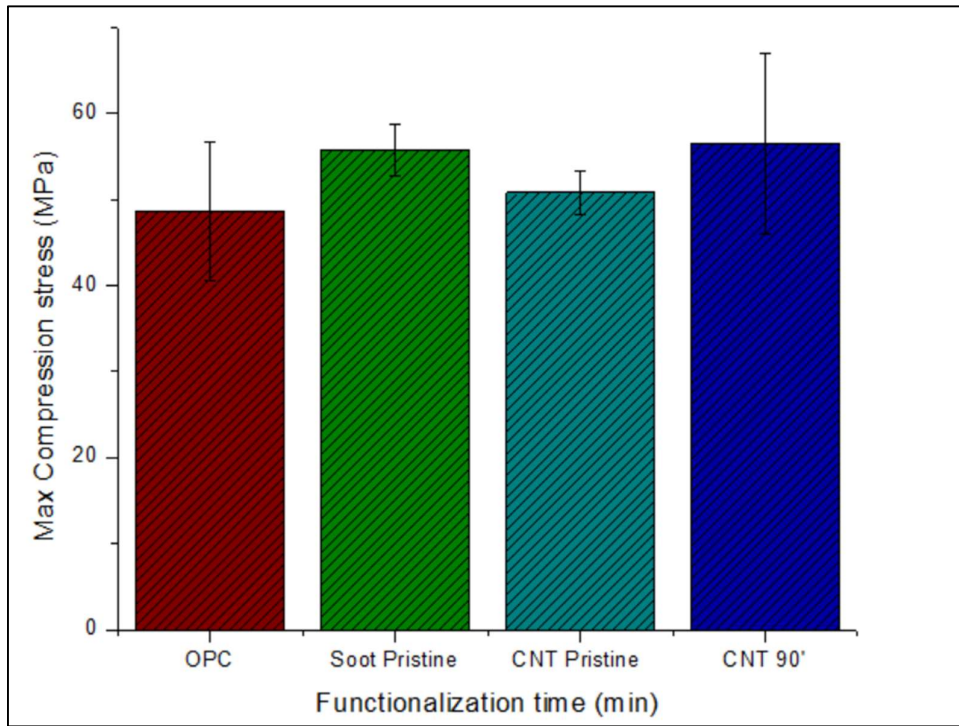


**Figure 5113.** Graph showing the comparison between graphene and CNTs in cement composites regarding the compression strength.

In general, regarding the mechanical properties of the composites, including 0,1% on cement volume of graphene-like nanoparticles inside the cement matrix seems to bring a higher enhancement concerning both the flexural and compression strengths.

## 8. CONCLUSIONS

The main goal of this work is was to analyze the influence of the acidic functionalization process for carbon nanotubes inside a cement-based composite, by examining 6 different CNTs-cement composite samples in which the nanotubes were functionalized for different times. Specifically, this work aimed to investigate the enhancement in mechanical and electrical properties of the CNT-cement composites by increasing the functionalization time by 15 minutes for each CNTs sample.

At the end of this work that was conducted in the DISAT and DISEG laboratories of the Politecnico di Torino, it can be asserted that an improvement both on mechanical and electrical properties on the composites was obtained. The effect of functionalization time on CNTs leads to an improvement both in the electrical conductivity and the flexural strength of the composites. These two aspects are probably improved first by the better dispersion of CNTs in the cement matrix, and second by the fact that increasing the number of oxygenated groups on the nanotubes surface, the interaction between the reinforcement (CNTs) and the matrix (cement) results stronger, allowing the creation of a better conductive path inside the cement and also increasing the composite strength under mechanical stresses. However, regarding the compression strength, the results didn't show a marked improvement by increasing the functionalization time of the CNTs, probably because of the formation of clusters that can decrease the effectiveness of the bonding between the reinforcement and the matrix.

In conclusion, the improvement of mechanical and electrical properties of the CNT-cement composites can lead to think that CNTs represent a very good alternative to the other carbon-based materials used as a reinforcement in the cement matrix. These results open the way to create a conductive cement with high mechanical properties that can be monitored during the lifetime of the structure in which is employed.

## LIST OF FIGURES

**FIGURE 1.** Structure of diamond lattice.

(<http://www.chm.bris.ac.uk/motm/diamond/diamonhdh.htm>)

**FIGURE 2.** Schematic representation of different type of Carbon nanotubes structures.

**FIGURE 3.** Representation of chiral vector and chiral angle for a SWCNT.

**FIGURE 4.** SEM image showing several walls of 5nm size for a MWCNT.

**FIGURE 5.** Scheme of a laser ablation method for the synthesis of carbon nanotubes.

**FIGURE 6.** Chemical Vapor Deposition process for the synthesis of MWCNTs.

**FIGURE 7.** CNTs applications in composite materials.

**FIGURE 8.** CNTs applications in microelectronic devices.

**FIGURE 9.** Main applications of CNTs in Energy storage (batteries and solar cells).

**FIGURE 10.** Full process of the production of Portland cement from limestone quarry to grinding.

**FIGURE 11.** Rate of Alite ( $C_3S$ ) hydration as a function of time given by isothermal calorimetry measurement.

**FIGURE 12.** Schematic representation of  $C_3S$  hydration.

**FIGURE 13.** Ideal hydration rate of  $C_3A$  in the presence of gypsum as a function of time.

**FIGURE 14.** Heat flow measured by isothermal conduction calorimetry.

**FIGURE 15.** Role of nano-additives in cement hydration process.

**FIGURE 16.** Overall cement hydration reaction with the presence of nanosilica.

**FIGURE 17.** Crack-bridging effect in cement CNTs composites. Monica J. Hanus , Andrew T. Harris, Progress in Materials Science. 58 (2013) 1056–1102.

**FIGURE 18.** Typical defects of a CNT surface after covalent functionalization.

**FIGURE 19.** Graphene-like reinforced cement composites under external loading.

**FIGURE 20.** Chemical Composition of Ordinary Portland Cement 52,5.

**FIGURE 21.** Scheme of the environment for the curing of the cement paste.

**FIGURE 22.** Scheme of a generic Thermogravimetric Analysis instrument.

**FIGURE 23.** Example of TGA curve for pristine Carbon Nanotubes. © 2021 Merck KGaA, Darmstadt, Germany.

**FIGURE 24.** Comparison of IR and Raman spectroscopy phenomena.

**FIGURE 25.** Scheme of a conventional Raman instrument.

**FIGURE 26.** Table showing the different functionalization times for the 6 CNTs samples in the 1 HNO<sub>3</sub> : 3H<sub>2</sub>SO<sub>4</sub> acidic solution.

**FIGURE 27.** Result of 30 minutes of sonication in the sulfunitric acid solution for CNTs.

**FIGURE 28.** Area of the cement sample interested by the current flow for the resistivity calculation.

**FIGURE 29.** Circular segment.

**FIGURE 30.** Geometry of the specimen used in the flexural strength test with the respective size and notch dimensions.

**FIGURE 31.** Extensometer configuration for the three-point test.

**FIGURE 32.** Picture of the compression test environment.

**FIGURE 33.** Graph showing TGA curves of carbon nanotubes functionalized at several sonication times.

**FIGURE 34.** Difference in decomposition starting temperature for: Pristine carbon nanotubes, carbon nanotubes sonicated for 30 minutes, carbon nanotubes sonicated for 75 minutes.

**FIGURE 35.** Comparison between Raman spectrum for nanotubes functionalized for 60 minutes (left) and nanotubes functionalized for 15 minutes (right).

**FIGURE 36.** Graph showing the ID/IG ratio for every functionalized CNT sample.

**FIGURE 37.** Values of max stress at breaking for CNT-cement samples with the relative error.

**FIGURE 38.** Bar chart reporting the values of Max stress for every samples of CNT-cement composite.

**FIGURE 39.** Graph showing every flexural test curve for all the CNT-concrete composite samples tested.

**FIGURE 40.** Table showing the compression strength for all the composite samples.

**FIGURE 41.** Comparison of compressive strength of all the CNT-cement samples tested by a compression machine.

**FIGURE 42.** Table with the values of Toughness evaluated by the flexural test.

**FIGURE 43.** Bar chart showing the difference in Fracture Energy for the CNT-composite samples.

**FIGURE 44.** Table with the resistivity comparison between functionalized CNT-cement composites.

**FIGURE 45.** Effect of functionalization time of CNTs on the resistivity of the composite.

**FIGURE 46.** Comparison of Flexural strength between the graphene-cement composite and CNT-cement composites.

**FIGURE 47.** Bar chart showing the flexural strength of the tested samples.

**FIGURE 48.** Table showing the toughness measured for the graphene-cement composite and the CNT-cement composite.

**FIGURE 49.** Bar chart showing the difference in toughness for the tested samples.

**FIGURE 50.** Comparison between the maximum compression stresses for graphene like-cement composites and CNT-cement composites.

**FIGURE 51.** Graph showing the comparison between graphene and CNTs in cement composites regarding the compression strength.

## BIBLIOGRAPHY

- [1] Rajendran, V. "*Materials science*". Tata McGraw-Hill Pub. p. 2.16. (2004).
- [2] Ashcroft, Neil W, Mermin, N. David. "Solid state physics". Holt, Rinehart and Winston. p. 76 (1976).
- [3] Delhaes, Pierre. "Polymorphism of carbon". In Delhaes, Pierre (ed.). *Graphite and precursors*. Gordon & Breach. pp. 1–24. (2000).
- [4] Iijima, S. Helical microtubules of graphitic carbon. *Nature* **354**, 56–58 (1991).
- [5] L.V. Radushkevich, V.M. Lukyanovich, O strukture ugleroda, obrazujucesja pri termiceskom razlozenii okisi ugleroda na zeleznom kontakte, *Zurn Fis. Chim.* 26 (1952) 88–95.
- [6] Mintmire, J.W.; Dunlap, B.I.; White, C.T. (3 February 1992). "Are fullerene tubules metallic?". *Phys. Rev. Lett.* 68 (5): 631–634.
- [7] Yu, M.; Lourie, O; Dyer, MJ; Moloni, K; Kelly, TF; Ruoff, RS (28 January 2000). "*Strength and Breaking Mechanism of Multiwalled Carbon Nanotubes Under Tensile Load*". *Science*. 287 (5453): 637–640
- [8] Das, Sudip (March 2013). "*A review on Carbon nano-tubes – A new era of nanotechnology*". *International Journal of Emerging Technology and Advanced Engineering*. 3 (3): 774–781.
- [9] Banu Abdallah, Mohammad Najlah, *Advances in Medical and Surgicla Engineering, from Carbon Nanotubes drug delivery system for cancer treatment* (2015)
- [10] Cumings, J.; Zettl, A. (2000). "*Low-Friction Nanoscale Linear Bearing Realized from Multiwall Carbon Nanotubes*". *Science*. 289 (5479): 602–604.
- [11] S. Cui, P. Scharff, C. Siegmund, D. Schneider, K. Risch, S. Klotzer, L. Spiess, H. Romanus, J. Schawohl, *J. Carbon* 42 (2004) 931.

- [12] A. Thess, R. Lee, P. Nikolaev, H. Dai, P. Petit, J. Robert, C. Xu, Y.H. Lee, S.G. Kim, A.G. Rinzler, D.T. Colbert, G.E. Scuseria, D. Tomanek, J.E. Fischer, R.E. Smalley, *Science* 273 (1996) 483.
- [13] H. Dai, *Surface Science* 500 (2002) 218.
- [14] M. Kumar, Y. Ando, *J. Nanoscience Nanotechnologies* 10 (2010) 3739.
- [15] Q. Zhao, T. Jiang, C. Li, H. Yin, *Direct Growth of Carbon Nanotubes on Metal Supports by Chemical Vapor Deposition*, *Ind Engineering Chemistry* 17 (2011) 218.
- [16] A. Govindaraj, C.N.R. Rao, *Pure Applied Chemistry* 74 (2002) 1571.
- [17] Z.F. Ren, Z.P. Huang, J.W. Xu, J.H. Wang, P. Bush, M.P. Seigal, P.N. Provencio, *Science* 282 (1998) 1105.
- [18] M. Lan, G. Fan, Q. Chen, F. Li, *J. Ind. Eng. Chem.* (2013), <http://dx.doi.org/10.1016/j.jiec.2013.07.042>.
- [19] K.Y. Lee, W.M. Yeoh, S.P. Chai, S. Ichikawa, A.R. Mohamed, *J. Ind. Eng. Chem.* 18 (2012) 1504.
- [20] J.S. Kim, Y.W. Jang, I.T. Im, *J. Ind. Eng. Chem.* 19 (2013) 1501.
- [21] Bingshe Xu, Li T, Liu X, Lin X, Li J, "Growth of well-aligned carbon nanotubes in a plasma system using ferrocene solution in ethanol". *Thin Solid Films* 515:6726–6729 (2007).
- [22] Point S, Minea T, Besland M-P, Granier A, "Characterization of carbon nanotubes and carbon nitride nanofibers synthesized by PECVD". *Eur Phys J Appl Phys* 34:157–163 (2006).
- [23] Khan MI, Qamar A, Shabbir F, Shoukat R, "Design, development and implementation of Low power and high-speed A/D converter in submicron CMOS technology". *Microsyst Technol* 23(12):6005–6014, (2017).
- [24] M. D. Lima et al., *Science* 331, 51 (2011).
- [25] N. Behabtu et al., *Science* 339, 182 (2013).
- [26] Takashi Kashiwagi, Fangming Du, Jack F Douglas, Karen I Winey, Richard H Harris Jr, John R Shields. *Nanoparticle networks reduce the flammability of polymer nanocomposites*. *Natural Materials* (2005).
- [27] Alexandre Beigbeder, Philippe Degee, Sheelagh L Conlan, Robert J Mutton, Anthony S Clare, Michala E Pettitt, Maureen E Callow, James A Callow, Philippe Dubois. *Preparation and characterisation of silicone-based coatings filled with carbon nanotubes and natural sepiolite and their application as marine fouling-release coatings*. *Biofouling* (2008).
- [28] Zhuangchun Wu, Zhihong Chen, Xu Du, Jonathan M Logan, Jennifer Sippel, Maria Nikolou, Katalin Kamaras, John R Reynolds, David B Tanner, Arthur F Hebard, Andrew G Rinzler. *Transparent, conductive carbon nanotube films*. *Science* (2004)
- [29] S. De, J. N. Coleman, *The effects of percolation in nanostructured transparent conductors* *MRS Bull.* 36, 774 (2011).
- [30] Aaron D. Franklin, Siyuranga O. Koswatta, Damon B. Farmer, Joshua T. Smith, Lynne Gignac, Chris M. Breslin, Shu-Jen Han, George S. Tulevski, Hiroyuki Miyazoe, Wilfried Haensch, and Jerry

Tersof. *Carbon Nanotube Complementary Wrap-Gate Transistors*. IBM T. J. Watson Research Center, Yorktown Heights, New York 10598, United States. (2013)

[31] Qing Cao, John A. Rogers. *Ultrathin Films of Single-Walled Carbon Nanotubes for Electronics and Sensors: A Review of Fundamental and Applied Aspects 1*

[32] Johannes Vanpaemel, Masahito Sugiura, Yohan Barbarin, Stefan De Gendt, Zsolt Tökei, Philippe M Vereecken, Marleen H van der Veen *Growth and integration challenges for carbon nanotube interconnects*, *Microelectronic engineering*, p 188-193.

[33] Lavagna, L.; Meligrana, G.; Gerbaldi, C.; Tagliaferro, A.; Bartoli, M. "Graphene and Lithium-Based Battery Electrodes: A Review of Recent Literature". *Energies*, 13, 4867 (2020).  
<https://doi.org/10.3390/en13184867>

[34] Kara Evanoff Javed Khan Alexander A. Balandin Alexandre Magasinski W. Jud Ready Thomas F. Fuller Gleb Yushin, *Towards Ultrathick Battery Electrodes: Aligned Carbon Nanotube – Enabled Architecture*. *Advanced Materials*, p 533-537 (2012)

[35] Chiaki Sotowa, Gaku Origi, Masataka Takeuchi, Yashiyuki Nishimura, Kenji Takeuchi, In Young Jang, Yong Jung Kim, Takuya Hayashi, Yoong Ahm Kim, *The Reinforcing Effect of Combined Carbon Nanotubes and Acetylene Blacks on the Positive Electrode of Lithium-Ion Batteries*, *ChemSusChem*, p 911-915 (2008)

[36] Nathaniel M. Gabor, Zhaohui Zhong, Ken Bosnick, Jiwoong Park, Paul L. McEuen, *Extremely Efficient Multiple Electron-Hole Pair Generation in Carbon Nanotube Photodiodes*, *Science*, Vol 325 (2009)

[37] Chad D. Vecitis, Guandao Gao, Han Liu *Electrochemical Carbon Nanotube Filter for Adsorption, Desorption, and Oxidation of Aqueous Dyes and Anions*, *The Journal of Physical Chemistry*, p 3621-3629 (2011)

[38] Jason K. Holt, Hyung Gyu Park, Yinmin Wang<sup>1</sup>, Michael Stadermann<sup>1</sup>, Alexander B. Artyukhin, *Fast Mass Transport Through Sub-2-Nanometer Carbon Nanotubes*

[39] Daniel A. Heller, Hong Jin, Brittany M. Martinez, Dhaval Patel, Brigid M. Miller, Tsun-Kwan Yeung, Prakrit V. Jena, Claudia Höbartner, Taekjip Ha, Scott K. Silverman. *Multimodal optical sensing and analyte specificity using single-walled carbon nanotubes*, *Nature Nanotechnology*, p 114-120 (2009).

[40] Alberto Bianco, Kostas Kostarelos, Charalambos D. Partidos, Maurizio Prato. *Biomedical applications of functionalised carbon nanotubes* (2005).

[41] Wissenschaftliche Berichte Fzka, M Achternbosch, K.-R Bräutigam, N Hartlieb, C Kupsch, U Richers, P Stemmermann, and M Gleis Umweltbundesamt. *Forschungszentrum Karlsruhe in der Helmholtz-Gemeinschaft Heavy Metals in Cement and Concrete Resulting from the Co-incineration of Wastes in Cement Kilns with Regard to the Legitimacy of Waste Utilisation*. Tech. rep. 2003

[42] Rajeb Salem Hwidi, Tengku Nuraiti Tengku Izhar, Farah Naemah Mohd Saad, Rajeb Salem Hwidi, Tengku Nuraiti Tengku Izhar, and Farah Naemah Mohd Saad. «Characterization of Limestone as Raw Material to Hydrated Lime». In: *E3SWC* 34 (2018),

- [43] G. Schumacher and L. Juniper. «Coal utilisation in the cement and concrete industries». In: *The Coal Handbook: Towards Cleaner Production*. Vol. 2. Elsevier Inc., Oct. 2013, pp. 387–426.
- [44] Britannica. Cement - Extraction and processing. url: <https://www.britannica.com/technology/cement-building-material/Extraction-andprocessing>
- [45] Whittaker. *The Effects of Prehydration on Cement Performance*.
- [46] P.M. Dove, N. Han, *Kinetics of mineral dissolution and growth as reciprocal microscopic surface processes across chemical driving force*, AIP Conference Proceedings, Vol. 916, 2007, pp. 215–234.
- [47] A.W. Adamson, A.P. Gast, *Physical Chemistry of Surfaces*, 6th Edition Wiley-Interscience, New York, 1997.
- [48] W.K. Burton, N. Cabrera, F.C. Frank, *The growth of crystals and the equilibrium structure of their surfaces*, Phil. Trans. R. Soc. Lond. A 243.
- [49] D. Kaschiev, G.M. van Rosmalen, Review: *nucleation in solutions revisited*, Cryst. Res. Technol. 38 (2003) 555–574.
- [50] F.M.M. Morel, *Principles of Aquatic Chemistry*, Wiley-Interscience, New York, 1983.
- [51] H. F. W. Taylor. *The Effects of Prehydration on Cement Performance*.
- [52] Jessica Crees. *Implementing Change in an SME*. In: *The Role of Enterprise Systems - IS Practices for SME Success*. Ed. by Jessica Crees and Richard Self. Vol. 26. 1-2. 2013.
- [53] E.M. Gartner, J.F. Young, D.A. Damidot, I. Jawed, *Hydration of portland cement*, in: J. Bensted, P. Barnes (Eds.), *Structure and Performance of Cements*, 2<sup>nd</sup> Edition, Spon Press, New York, 2002, pp. 57–113.
- [54] M.M. Costoya, Effect of particle size on the hydration kinetics and microstructural development of tricalcium silicate, PhD dissertation, École Polytechnique Fédérale de Lausanne, Lausanne, Switzerland, 2008.
- [55] Jeffrey J. Thomas, Sam Ghazizadeh, and Enrico Masoero. «Kinetic mechanisms and activation energies for hydration of standard and highly reactive forms of  $\beta$ -dicalcium silicate (C2S)». In: *Cement and Concrete Research* 100 (Oct. 2017), pp. 322–328.
- [56] K.L. Scrivener, P. Juilland, P.J.M. Monteiro, *Advances in understanding hydration of Portland cement*, Cem. Concr. Res. 78 (2015) 38–56
- [57] J. Plank, D. Zhimin, H. Keller, F. Hössle, W. Seidl, *Fundamental mechanisms for polycarboxylate intercalation into C3A hydrate phases and the role of sulfate present in cement*, Cem. Concr. Res. 40 (1) (2010) 45–57.
- [58] A. Habbaba, Z. Dai, J. Plank, *Formation of organo-mineral phases at early addition of superplasticizers: the role of alkali sulfates and C3A content*, Cem. Concr. Res. 59 (2014) 112–117.
- [59] L. Black, C. Breen, J. Yarwood, C. Deng, J. Phipps, G. Maitland, *Hydration of tricalcium aluminate (C3A) in the presence and absence of gypsum—studied by Raman spectroscopy and X-ray diffraction*, J. Mater. Chem. 16 (13) (2006) 1263–1272.

- [60] J. Pommersheim, J. Chang, *Kinetics of hydration of tricalcium aluminate*, Cem. Concr. Res. 16 (3) (1986) 440–450.
- [61] H.N. Stein, *Mechanism of the hydration of  $3\text{CaO}\cdot\text{Al}_2\text{O}_3$* , J. Appl. Chem. 13 (5) (1963) 228–232.
- [62] G.C. Bye, *Portland Cement: Composition, Production and Properties*, Thomas Telford, 1999.
- [63] H. Minard, S. Garrault, L. Regnaud, A. Nonat, Mechanisms and parameters controlling the tricalcium aluminate reactivity in the presence of gypsum, Cem. Concr. Res. 37 (10) (2007) 1418–1426.
- [64] A. Quennoz, K.L. Scrivener, *Hydration of C3A–gypsum systems*, Cem. Concr. Res. 42 (7) (2012) 1032–1041.
- [65] A. Quennoz, *Hydration of C3A With Calcium Sulfate Alone and in the Presence of Calcium Silicate* (PhD Thesis), EPFL, 2011, <https://infoscience.epfl.ch/record/164029>.
- [66] Meller N, Hall C, Crawshaw J. *ESEM evidence for through-solution transport during brownmillerite hydration*. *J Mater Sci*. 2004; 39(21): 6611–4.
- [67] Rose J, Bénard A, El Mrabet S, Masion A, Moulin I, Briois V, et al. *Evolution of iron speciation during hydration of  $\text{C}_4\text{AF}$* . *Waste Manage*. 2006; 26(7): 720–4.
- [68] Jung, S.; Oh, S.; Kim, S.-W.; Moon, J.-H. *Effects of CNT Dosages in Cement Composites on the Mechanical Properties and Hydration Reaction with Low Water-to-Binder Ratio*. *Appl. Sci*. 2019, 9, 4630
- [69] Wang, B.; Pang, B. *Properties improvement of multiwall carbon nanotubes-reinforced cement-based composites*. *J. Compos. Mater*. 2019, 54, 2379–2387.
- [70] Cui, H.; Yang, S.; Memon, S.A. *Development of carbon nanotube modified cement paste with microencapsulated phase-change material for structural-functional integrated application*. *Int. J. Mol. Sci*. 2015, 16, 8027–8039.
- [71] Alatawna, A.; Birenboim, M.; Nadiv, R.; Buzaglo, M.; Peretz-Damari, S.; Peled, A.; Regev, O.; Sripada, R. *The effect of compatibility and dimensionality of carbon nanofillers on cement composites*. *Constr. Build. Mater*. 2020, 232, 117141.
- [72] Baoguo Han, Shengwei Sun, Siqi Ding, Liqing Zhang, Xun Yu, Jinping Ou, *Innovative Developments of Advanced Multifunctional Nanocomposites: Part A*. (2015) 69–81
- [73] Baoguo Han, Shengwei Sun, Siqi Ding, Liqing Zhang, Xun Yu, Jinping Ou, *Electrostatic self-assembled carbon nanotube / nano carbon black composite fillers reinforced cement-based materials with multifunctionality*. (2015)
- [74] M.Hanus, A. Harris, *Nanotechnology innovations for the construction industry* August 2013, Progress in Materials Science :1056–1102
- [75] J. Makar, J. Margeson and J. Luh, “*In Carbon Nanotube/ Cement Composites-Early Results and Potential Applications*,” *Proceedings of the 3rd International Conference on Construction Materials: Performance, Innovations and Structural Implications*, Vancouver, 22-24 August 2005, pp. 1-10.
- [76] Maria S. Konsta-Gdoutos, Zoi S. Metaxa, Surendra P. Shah, *Highly dispersed carbon nanotube reinforced cement-based materials*, Cement and Concrete Research. 40 (2010) 1052–1059.

- [77] Chen, R. J.; Zhang, Y.; Wang, D. & Dai, H. (2001). *Noncovalent Sidewall Functionalization of Single-walled carbon nanotubes for protein immobilization*. J. Am. Chem. Soc. 123, 3838–3839.
- [78] Hirsch, A. (2002). *Functionalization of Single-Walled Carbon Nanotubes*. Angew, Chem, Int. Ed. 41, (11), 1853-1859.
- [79] Bianco, A.; Prato, M.; Kostarelos, K. & Bianco, A. (2008). *Functionalized Carbon Nanotubes in Drug Design and Discovery*. Acc. Chem. Res. 41, (1), 60-68.
- [80] Kelly, K.F.; Chiang, I.W.; Mickelson, E.T., et al. (1993). *Insight into the mechanism of sidewall functionalization of single-walled nanotubes: an STM study*. Chem. Phys. Lett. 313, 445–450.
- [81] Chen, J.; Hamon, M.A.; Hu, H.; Chen, Y.; Rao, A.M.; Eklund, P.C.; Haddon, R.C. (1998). *Solution Properties of Single-Walled Carbon Nanotubes*. Science 282, (5386), 95- 98.
- [82] D.K.Chattopadhyay, Dean C.Webster *Thermal stability and flame retardancy of polyurethanes*. Department of Coatings & Polymeric Materials, North Dakota State University, Fargo, ND 58105, USA
- [83] Gardiner, D.J. (1989). *Practical Raman spectroscopy*. Springer-Verlag. ISBN 978-0-387-50254-0.
- [84] McCreery, Richard L. (2000). *Raman spectroscopy for chemical analysis*. New York: John Wiley & Sons. ISBN 0471231878.
- [85] Elliott, Anastasia B. S.; Horvath, Raphael; Gordon, Keith C. (2012). *"Vibrational spectroscopy as a probe of molecule-based devices"*. Chem. Soc. Rev. 41 (5): 1929–1946.
- [86] Luca Lavagna, Daniele Massella, Matteo Pavese, *"Preparation of hierarchical material by chemical grafting of carbon nanotubes onto carbon fibers"*, Diamond and Related Materials, Volume 80, 2017, Pages 118-124, ISSN 0925-9635, <https://doi.org/10.1016/j.diamond.2017.10.013>.